

**BRNO UNIVERSITY OF TECHNOLOGY**

**Faculty of Electrical Engineering  
and Communication**

**MASTER'S THESIS**

**Brno, 2022**

**Bc. Martin Světlík**



# BRNO UNIVERSITY OF TECHNOLOGY

VYSOKÉ UČENÍ TECHNICKÉ V BRNĚ

## FACULTY OF ELECTRICAL ENGINEERING AND COMMUNICATION

FAKULTA ELEKTROTECHNIKY  
A KOMUNIKAČNÍCH TECHNOLOGIÍ

## DEPARTMENT OF POWER ELECTRICAL AND ELECTRONIC ENGINEERING

ÚSTAV VÝKONOVÉ ELEKTROTECHNIKY A ELEKTRONIKY

# THERMAL MODEL OF OUTER ROTOR PERMANENT MAGNET SYNCHRONOUS MACHINE

TEPELNÝ MODEL SYNCHRONNÍHO STROJE S PERMANENTNÍMI MAGNETY A VNĚJŠÍM ROTOREM

## MASTER'S THESIS

DIPLOMOVÁ PRÁCE

### AUTHOR

AUTOR PRÁCE

**Bc. Martin Světlík**

### SUPERVISOR

VEDOUCÍ PRÁCE

**Ing. Marek Toman**

**BRNO 2022**

# Master's Thesis

Master's study program **Power Electrical and Electronic Engineering**

Department of Power Electrical and Electronic Engineering

**Student:** Bc. Martin Světlík

**ID:** 206814

**Year of  
study:** 2

**Academic year:** 2021/22

**TITLE OF THESIS:**

## **Thermal Model of Outer Rotor Permanent Magnet Synchronous Machine**

**INSTRUCTION:**

1. Study and describe methods of loss calculations and thermal modeling of electrical machines.
2. Study and describe optimization methods suitable for estimation of thermal parameters of electrical machines.
3. Using the studied methods, optimize parameters of a thermal model of outer rotor permanent magnet synchronous machine and compute temperatures of individual machine parts.
4. Compare calculated results with measured data.

The work is carried out in collaboration with JKU - Johannes Kepler Universität Linz and the LCM - Linz Center of Mechatronics.

**RECOMMENDED LITERATURE:**

- [1] PYRHONEN, Juha, Tapani JOKINEN a Valéria HRABOVCOVÁ. Design of rotating electrical machines. Second Edition. WILEY, 2014.
- [2] CENGEL Yunus a Afshin GHAJAR. Heat and mass transfer. Fifth edition. McGraw hill education, 2015.
- [3] WÖCKINGER Daniel, Gerd BRAMERDORFER a Stephan DREXLER, aj.: Measurement-Based Optimization of Thermal Networks for Temperature Monitoring of Outer Rotor PM Machines. IEEE, 2020.

**Date of project  
specification:** 7.2.2022

**Deadline for  
submission:** 22.5.2022

**Supervisor:** Ing. Marek Toman

**doc. Ing. Ondřej Vitek, Ph.D.**  
Chair of study program board

**WARNING:**

The author of the Master's Thesis claims that by creating this thesis he/she did not infringe the rights of third persons and the personal and/or property rights of third persons were not subjected to derogatory treatment. The author is fully aware of the legal consequences of an infringement of provisions as per Section 11 and following of Act No 121/2000 Coll. on copyright and rights related to copyright and on amendments to some other laws (the Copyright Act) in the wording of subsequent directives including the possible criminal consequences as resulting from provisions of Part 2, Chapter VI, Article 4 of Criminal Code 40/2009 Coll.

## **ABSTRACT**

This thesis deals with permanent magnet synchronous machines. Special attention is paid to machines with an outer rotor. The first part describes the losses occurring in the machine, their distribution, and subsequent analysis. Then the heat transfer mechanisms are described, with a description of their application in the field of electrical machines. Among other things, this work focuses on methods suitable for the optimization of heat network parameters. These methods are further applied to the optimization mentioned above of these parameters. The results of calculations obtained using the previously mentioned optimization methods are evaluated and compared with measured data in the last chapter. These results are compared in terms of approximation to the measured data, computational time, and computational effort.

## **KEYWORDS**

Cooling methods, losses analysis, methods of optimization, optimization of parameters, outer rotor machines, thermal model, thermal network

## **ABSTRAKT**

Tato práce se zabývá synchronními stroji s permanentními magnety. Zvláštní pozornost je věnována strojům s vnějším rotorem. V první části jsou popsány ztráty vznikající ve stroji, jejich rozdělení a následná analýza. Dále jsou zde popsány mechanismy přenosu tepla, s popisem jejich využití v oblasti elektrických strojů. Mimo jiné je tato práce zaměřena i na metody vhodné pro optimalizaci parametrů tepelné sítě. Tyto metody jsou dále použity pro již zmíněnou optimalizaci těchto parametrů. V poslední kapitole jsou zhodnoceny výsledky výpočtů získaných s využitím dříve uvedených optimalizačních metod a jejich porovnání s naměřenými daty. Tyto výsledky jsou zde porovnány z hlediska přiblížení se naměřeným datům, výpočetního času a výpočetní náročnosti.

## **KLÍČOVÁ SLOVA**

Způsoby chlazení, analýza ztrát, optimalizační metody, optimalizace parametrů, stroj s vnějším rotorem, teplný model, tepelná síť

## ROZŠÍŘENÝ ABSTRAKT

Tato diplomová práce se zabývá tepelným modelem synchronního stroje s permanentními magnety a vnějším rotorem. Pro správné sestavení tepelného modelu je nutná analýza ztrát stroje. Tyto ztráty generují teplo v oblastech jejich vzniku. Vzniklé teplo je nutné odvádět mimo stroj a to buď do jeho okolí nebo do ostatních částí soustavy, ve které je tento stroj používán. Sestavený tepelný model zohledňuje oblasti, ve kterých dochází ke generování těchto ztrát tak, aby odpovídal vlastnostem analyzovaného stroje.

První kapitola se zabývá rozdělením synchronních strojů do jednotlivých skupin podle konstrukce. Hlavními skupinami synchronních strojů jsou cizebuzené synchronní stroje, reluktanční synchronní stroje a synchronní stroje s permanentními magnety. Dále je zde popsán obecný princip funkce synchronních strojů včetně ekvivalentního obvodu a fázorového diagramu.

V druhé kapitole jsou popsány již zmíněné ztráty elektrického synchronního stroje. Jejich rozdělení principy vzniku jednotlivých typů ztrát a způsob jejich výpočtu. Jelikož je dále v této práci analyzován stroj s nominálními otáčkami  $7500 \text{ min}^{-1}$  jsou v této kapitole uvedeny i mechanické ztráty, včetně způsobu jejich výpočtu.

Třetí kapitola se dotýká tématu přenosu tepla. Jsou zde popsány jednotlivé mechanismy jeho přenosu včetně způsobu chlazení elektrických strojů. V rámci popisu chlazení jsou popsány způsoby, kterými je možné modelovat tepelný odpor konvekcí a závislosti na otáčkách rotoru. Tento způsob je zde uveden, jelikož analýza tohoto typu přenosu tepla je velmi komplexní. Zároveň se jedná o nezanedbatelný způsob, jakým dochází v točivých strojích k přenosu tepla. Jednotlivé typy závislostí jsou zde graficky zobrazeny v závislosti na otáčkách.

Následující kapitola popisuje metody, které jsou použity pro optimalizaci parametrů tepelného modelu analyzovaného stroje. Tyto metody umožňují optimalizovat model stroje tak, aby co nejvíce odpovídal realitě. Díky optimalizovanému modelu stroje je možné matematicky ověřit případné změny provedené v jeho návrhu a to bez nutnosti výroby velkého množství laboratorních vzorků.

V páté kapitole je popsán analyzovaný stroj. Jeho jmenovité parametry, oblast ve které je tento stroj provozován a teploty naměřené při definovaném duty-cyclu. Dále je zde uvedena tepelná síť tohoto stroje.

Šestá kapitola popisuje praktické použití optimalizačních metod a graficky znázorňuje jejich výsledky v porovnání s měřenými teplotami. V neposlední řadě také uvádí vstupní data použité v jednotlivých metodách. Dále jsou zde uvedeny matematické filtry použité pro úpravu vstupních dat.

Poslední kapitola se zabývá porovnáním vypočtených dat s naměřenými.

SVĚTLÍK, Martin. *Thermal Model of Outer Rotor Permanent Magnet Synchronous Machine*. Brno: Brno University of Technology, Faculty of Electrical Engineering and Communication, Department of Power Electrical and Electronic Engineering, 2022, 78 p. Master's Thesis. Advised by Ing. Marek Toman

# Author's Declaration

**Author:** Bc. Martin Světlík  
**Author's ID:** 206814  
**Paper type:** Master's Thesis  
**Academic year:** 2021/22  
**Topic:** Thermal Model of Outer Rotor Permanent Magnet Synchronous Machine

I declare that I have written this paper independently, under the guidance of the advisor and using exclusively the technical references and other sources of information cited in the paper and listed in the comprehensive bibliography at the end of the paper.

As the author, I furthermore declare that, with respect to the creation of this paper, I have not infringed any copyright or violated anyone's personal and/or ownership rights. In this context, I am fully aware of the consequences of breaking Regulation § 11 of the Copyright Act No. 121/2000 Coll. of the Czech Republic, as amended, and of any breach of rights related to intellectual property or introduced within amendments to relevant Acts such as the Intellectual Property Act or the Criminal Code, Act No. 40/2009 Coll. of the Czech Republic, Section 2, Head VI, Part 4.

Brno .....

.....

author's signature\*

---

\*The author signs only in the printed version.

## ACKNOWLEDGEMENT

I would like to thank the advisor of my thesis, Ing. Marek TOMAN for his patience, right guidance, and expert consultation regarding my work.

Furthermore, I would like to thank Assoc.Prof.Dr. Gerd BRAMERDORFER for the opportunity to do an internship at JKU Linz, which have been Financed by: Federal Ministry of Educaton, Science and Research (BMBWF), Awarding organisation: OeAD – Austria´s Agency for Educaton and Internatonalisaton, Mobility Programmes, Bilateral and Multilateral Cooperation.

This work has been supported by the COMET-K2 Center of the Linz Center of Mechatronics (LCM) funded by the Austrian federal government and the federal state of Upper Austria.

Last but not least, my great thanks go to DI Daniel WÖCKINGER, who devoted a lot of time and provided me with valuable information and advice in thermal calculations.

Many thank also go to my family, who supported me throughout my studies.



# Contents

<b>Introduction</b>	<b>14</b>
<b>1 Synchronous machine</b>	<b>15</b>
1.1 Construction of synchronous machine . . . . .	16
1.1.1 Permanent magnet synchronous machine with inner rotor . . .	17
1.1.2 Permanent magnet synchronous machine with outer rotor . . .	18
1.2 Principle of synchronous machine function . . . . .	18
1.2.1 Equivalent circuit of PMSM . . . . .	19
1.2.2 Phasor diagram of PMSM . . . . .	21
1.2.3 Torque of PMSM . . . . .	22
<b>2 Losses in permanent magnet synchronous machine</b>	<b>23</b>
2.1 Stator copper losses . . . . .	24
2.2 Stator magnetic losses . . . . .	24
2.2.1 Hysteresis losses . . . . .	25
2.2.2 Eddy current losses in a laminated material . . . . .	25
2.2.3 Excess losses . . . . .	26
2.3 Rotor losses . . . . .	26
2.4 Mechanical losses . . . . .	27
2.4.1 Bearing losses . . . . .	27
2.4.2 Gas frictional losses . . . . .	27
<b>3 Heat transfer</b>	<b>30</b>
3.1 Conduction . . . . .	30
3.2 Convection . . . . .	32
3.2.1 Natural convection . . . . .	32
3.2.2 Forced convection . . . . .	33
3.3 Radiation . . . . .	33
3.4 Machine cooling . . . . .	34
3.5 Modelling of speed-dependent resistances . . . . .	35
3.5.1 Heat transfer coefficient derivation . . . . .	37
<b>4 Optimizing methods</b>	<b>42</b>
4.1 Genetic algorithm . . . . .	42
4.1.1 Selection rules . . . . .	42
4.1.2 Crossover rules . . . . .	43
4.1.3 Mutation rules . . . . .	43
4.2 Decision tree . . . . .	44

4.2.1	Nodes . . . . .	45
4.2.2	Branches . . . . .	45
4.2.3	Splitting . . . . .	46
4.2.4	Stopping . . . . .	46
4.2.5	Pruning . . . . .	46
<b>5</b>	<b>Analysed machine</b>	<b>47</b>
5.1	Thermal network . . . . .	49
<b>6</b>	<b>Thermal analysis</b>	<b>50</b>
6.1	Application of the genetic algorithm . . . . .	50
6.2	Application of decision tree . . . . .	54
6.2.1	Data preparing . . . . .	54
<b>7</b>	<b>Comparison of calculated results and measured data</b>	<b>61</b>
7.1	Data evaluation . . . . .	61
	<b>Conclusion</b>	<b>64</b>
	<b>Bibliography</b>	<b>65</b>
	<b>Symbols and abbreviations</b>	<b>70</b>
	<b>List of appendices</b>	<b>77</b>
<b>A</b>	<b>Datasheet of analyzed machine</b>	<b>78</b>

# List of Figures

1.1	Categorization of synchronous machine types . . . . .	15
1.2	Examples of permanent magnet synchronous machines rotors . . . . .	16
1.3	Types of synchronous machine rotors . . . . .	17
1.4	Examples of machines . . . . .	17
1.5	Cross section of PMSM with outer rotor . . . . .	18
1.6	Equivalent circuit of permanent magnet synchronous machine . . . . .	19
1.7	Phase diagram of permanent magnet synchronous machine . . . . .	21
2.1	Machine loss dividing . . . . .	23
2.2	Flow origins . . . . .	28
3.1	Heat transfer through the plane wall . . . . .	31
3.2	Heat transfer in the cylinder and cylindrical bar . . . . .	31
3.3	Natural convection . . . . .	33
3.4	Forced convection . . . . .	33
3.5	Linear and quadratic conduction heat resistances . . . . .	36
3.6	Heat transfer coefficient different $c_1$ , $c_2$ and $c_3$ . . . . .	37
3.7	Linear and quadratic heat transfer coefficients approximation . . . . .	39
3.8	Thermal resistances different $c_1$ , $c_2$ , $c_3$ and $S$ . . . . .	40
3.9	Linear and quadratic thermal resistances . . . . .	40
4.1	Selection rules . . . . .	43
4.2	Crossover rules . . . . .	43
4.3	Mutation rules . . . . .	43
4.4	Block scheme of generic algorithm . . . . .	44
4.5	Block diagram of decision tree . . . . .	45
5.1	Testing area . . . . .	47
5.2	Measured temperatures and duty cycle . . . . .	48
5.3	Thermal network . . . . .	49
6.1	Graphs based on linear heat transfer coeff. calculated by the GA . . . . .	51
6.2	Graphs based on quadratic heat transfer coeff. calculated by the GA . . . . .	52
6.3	Graphs calculated by genetic algorithm . . . . .	53
6.4	Example of moving average filter using . . . . .	55
6.5	Example of moving average filter using . . . . .	55
6.6	Example of exponential moving average filter using . . . . .	56
6.7	Quality of the decision tree learning for raw data . . . . .	57
6.8	Graphs calculated by decision tree using raw data . . . . .	57
6.9	Quality of the decision tree learning for MA filter . . . . .	58
6.10	Graphs calculated by decision tree using MA filtered data . . . . .	59
6.11	Quality of the decision tree learning for EMA filter . . . . .	59

6.12 Graphs calculated by decision tree using EMA filter . . . . . 60

# List of Tables

3.1	Table of variables . . . . .	41
5.1	Table of machine nominal values . . . . .	47
5.2	Table of started conductivity resistances . . . . .	49
6.1	Table of optimized linear and quadratic heat transfer coefficients . . .	50
6.2	Table of optimized heat transfer coefficients . . . . .	52
6.3	Table of features used for the decision tree creating . . . . .	54
7.1	Table of mean squared errors in single nodes . . . . .	61
7.2	Table of mean squared errors in single nodes . . . . .	62

# Introduction

Synchronous machines (SMs) are universal machines to alternating-current (AC). Moreover, the role of synchronous machines is increasing in the industry nowadays. It is because it is used for motor drive applications and thanks to the development of power electronics.

Synchronous motor drives are also used in systems requiring high power, such as ventilator systems, large pumping stations, or big ship propulsion systems. Salient-pole or non-salient pole machines for these applications are usually used. Non-salient pole machines are used for high-speed applications like pumps, and salient pole machines are used for low-speed applications like the pressers. Another reason for their frequent use is the continuous capability to compensate for the reactive power.

Currently, synchronous reluctance machines are more used than capability to replace induction machines or drives with synchronous machines and inverters in commercial applications. These machines connect the capability of induction machines starting without an inverter and synchronous machine torque-speed characteristic and efficiency into one compact synchronous reluctance machine.

Permanent magnet synchronous machine with outer rotor is suitable for fan applications in the low-cost segment. Because the low price its using is very economical. Nevertheless, these machines must be designed to maximal using utility. That means over-dimensioned machines are not economic, but under-dimensioned machines have a very short lifetime. So the right dimensioning is very crucial.

A properly designed thermal network is a very powerful tool for machine designing. For the right dimensioning, it is crucial to estimate temperatures in the machine. It is possible to estimate the temperatures by using the LPTM (lumped parameters thermal network). One of the LPTN optimizing ways is the so-called genetic algorithm. This algorithm is described and used in this thesis.

Even the suitable dimensioned machine, in some cases, needs thermal controlling. One of the temperature monitoring ways is thermal sensors using. This way is especially in the low-cost sector disadvantageous. It is because evaluating the sensors and, in some cases, adapting the machine for the sensors is needed. So it is useful to use the real-time modeling of the machine's temperatures. This way of temperature control is cheaper and does not need any thermal sensors and adapting of the machine for these sensors.

The real-time modeling needs only inputs and DSP (digital signal processor) for temperature computing. The DSP uses only mathematics for temperature estimation. There are, of course, several ways of the mathematical estimation of the temperatures used by the DPS. One of these ways is to optimized LPTN, and the other is, for example, a decision tree. The named methods are used in this thesis.

# 1 Synchronous machine

This chapter describes the principle, construction, and division of the synchronous machine family. This thesis is focused mainly on a permanent magnet synchronous machine with an outer rotor. It is because the goal of this thesis is analyzing of this type of machine.

The family of the synchronous machines is shown in the picture 1.1. There are three main categories of synchronous machines in this picture. These categories are based on the ratio of quadrature axis (q-axis) and direct axis (d-axis) inductances. [1]

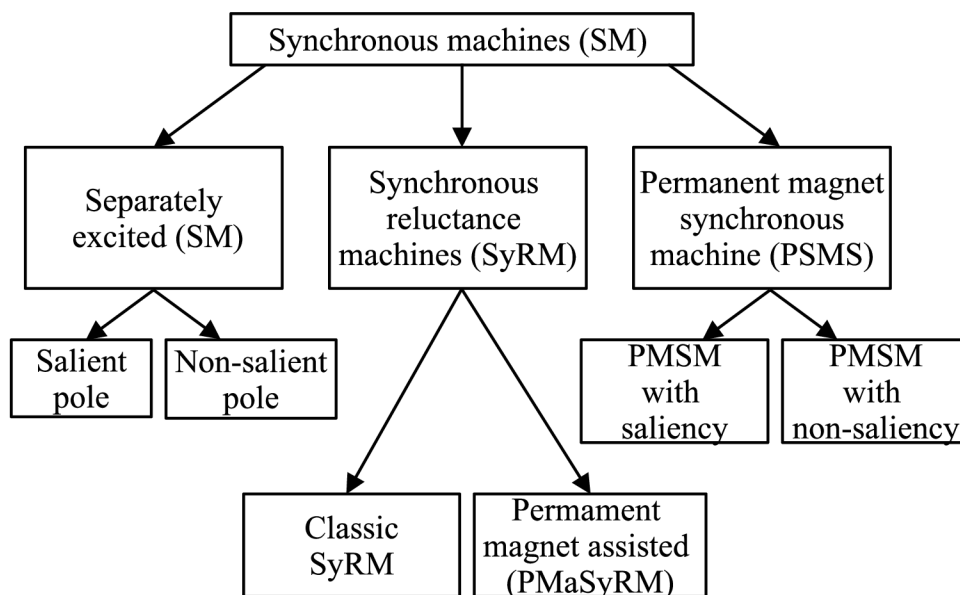


Fig. 1.1: Categorization of synchronous machine types

According to [1] the categorization of the two-axis electric machine is commonly used. It is because describing the machine's behavior to the two magnetic orientations is often very convenient. Usually, in the synchronous machine is a magnetic reluctance minor in the d-axis. That means the main part of flux is concentrated in this axis. On the other hand, on the q-axis synchronous machines have much more considerable magnetic reluctance than on the d-axis, so the magnetic flux is very low. Magnetic reluctance in the d-axis and q-axis might be same in some cases. Visualization of these axes can be seen in the figure 1.2, where parts a) and b) are examples of permanent magnet synchronous machines with saliency.

Reluctances in the q-axis and the d-axis are almost same in non-salient synchronous machines. That means there is no difference in the influence of the quadrature and direct magnetic flux, and therefore it does not matter the actual position of the stator and rotor. [2] Example of the machine types with an inner rotor is shown in part c) and with the outer rotor in the part d) of the figure 1.2

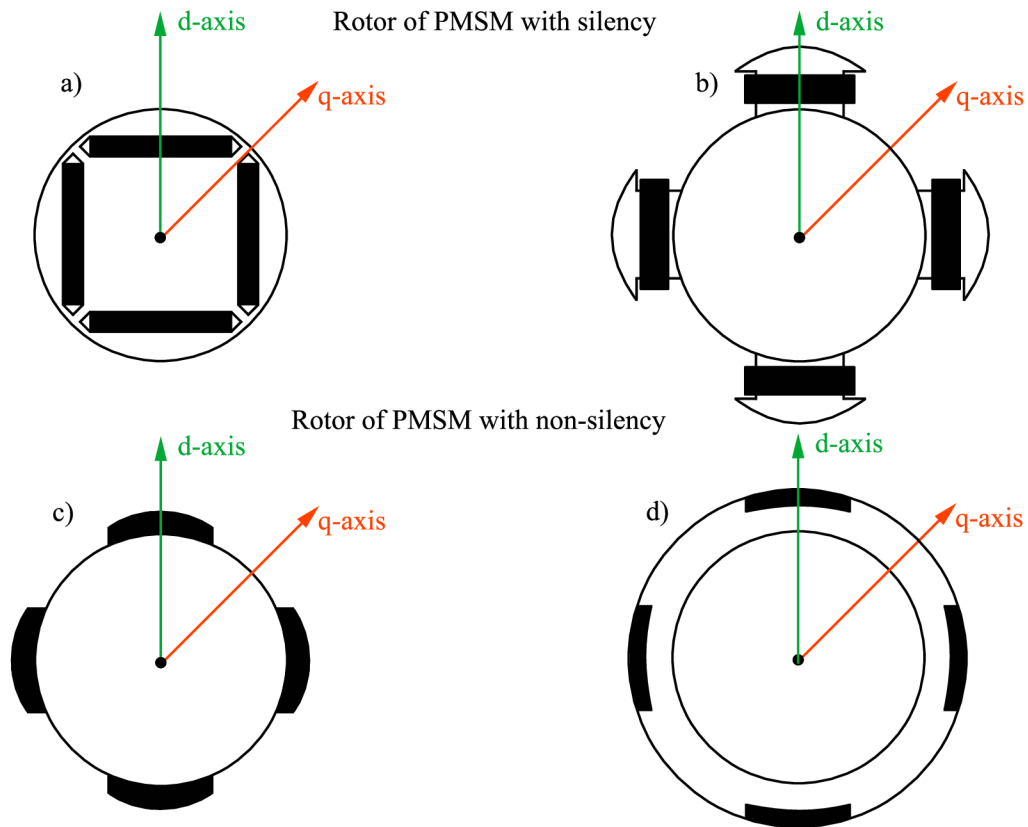


Fig. 1.2: Examples of permanent magnet synchronous machines rotors

## 1.1 Construction of synchronous machine

Synchronous machines consist of two main parts. These parts are the stator and rotor. The stator is a static part of the machine and consists of a frame, iron core, and winding. [3]

The iron core consists of two parts which are called yoke and teeth. This iron core is almost always divided into the stator plates. Dividing one massive part of the material into the many little sheets decreases eddy current losses. [1] The construction of stators is principally same in all types of synchronous machines. Only in the case of outer rotor synchronous machines is the stator located in the rotor and consists of the iron core and winding. A mounting flange replaces the frame. [4] These types of stators are shown in the picture 1.3



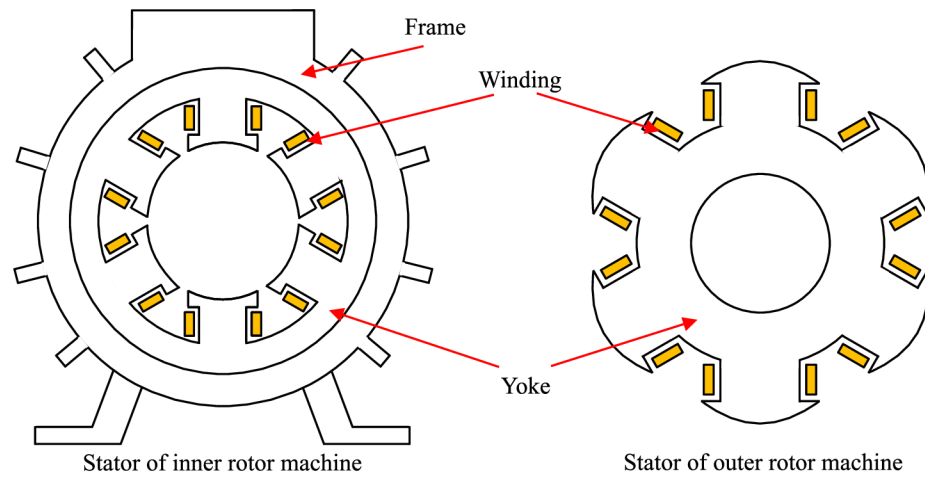


Fig. 1.3: Types of synchronous machine rotors

### 1.1.1 Permanent magnet synchronous machine with inner rotor

The rotor construction is based on the type of synchronous machine. In separately excited synchronous machines, the wound laminated rotors are used. Examples of these rotor types are shown in the figure 1.4. In synchronous reluctance machines, the same laminated rotors are used in the field of separately exciting synchronous machines. Nevertheless, these rotors are unwound, and some rotor teeth are removed. These unwound rotors are shown in the figure 1.4. In rotors of synchronous reluctance machines might also be used permanent magnets. These magnets are usually placed in the grooves. The construction of this type of rotor is shown in the figure 1.4. [7]

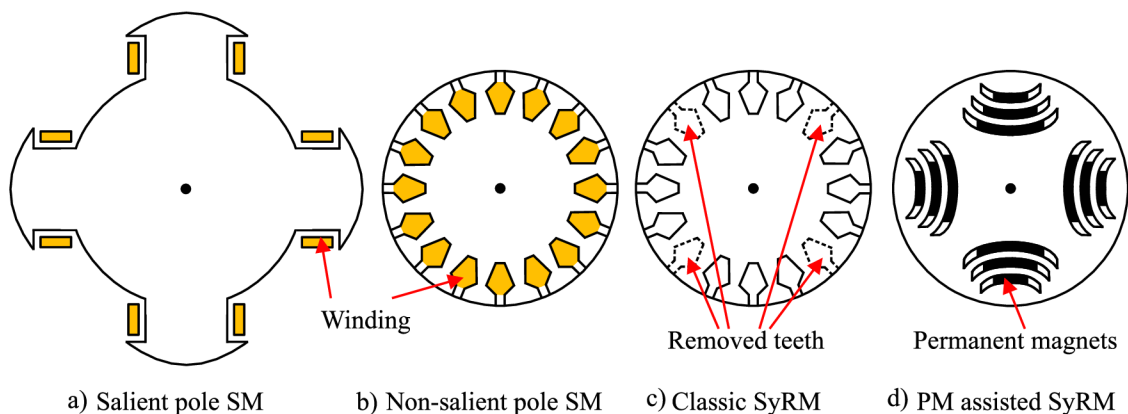


Fig. 1.4: Examples of separately excited and reluctance synchronous machines rotors

### 1.1.2 Permanent magnet synchronous machine with outer rotor

In this thesis, the primary attention is paid to permanent magnet synchronous machines with an outer rotor. An example of this type of rotor is shown in the figure 1.2 d). In the figure 1.5 the cross-section of the permanent magnet synchronous machine with the outer rotor is shown. This picture shows how the main parts of this machine are situated. Rotors used for this machine are not laminated but made from one material piece and look like a bell around the stator. This phenomenon is typical for all outer rotor machines.

The main benefits of outer rotor machines are high torque density, high output power, high efficiency, better rotor cooling, and an extensive speed range. On the other hand, the disadvantages are the large outer diameters of the machine, the eccentric load of used bearings, and worse stator cooling. These properties predispose this type of machine for use as wind generators, machine tools, fans, wheel drives, and so on. [5], [6]

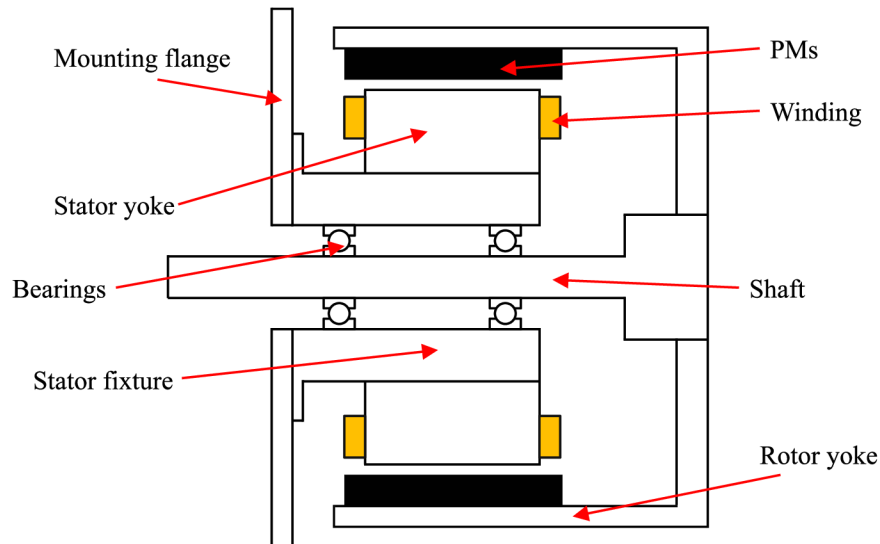


Fig. 1.5: Cross section of PMSM with outer rotor

## 1.2 Principle of synchronous machine function

The unique properties of all types of synchronous machines in steady-state are that the rotor's rotating speed and the spinning magnetic field produced by stator winding are the same. This phenomenon is called synchronous speed, which is why this group of machines is called synchronous machines. Synchronous machines can work in both generators and also motor mode.

### 1.2.1 Equivalent circuit of PMSM

Equivalent circuit of permanent magnet synchronous machines helps us understand its behaviour. Equivalent circuit shown in figure 1.6 is based on the equations for voltage in q-axis and d-axis. These equations are in the rotor reference frame in the following familiar form for the stator. [1] Voltage in the d-axis is defines

$$u_d = R_s i_d + \frac{d\psi_d}{dt} - \omega_r \psi_q \quad (1.1)$$

where  $R_s$  is stator resistance,  $i_d$  is current in the d-axis,  $\psi_d$  is flux linkage in the d-axis,  $t$  is time,  $\omega_r$  is angular velocity of rotor and  $\psi_q$  is flux linkage in the q-axis. The voltage in q-axis is defined by equation

$$u_q = R_s i_q + \frac{d\psi_q}{dt} + \omega_r \psi_d, \quad (1.2)$$

where  $i_q$  is current in the q-axis.

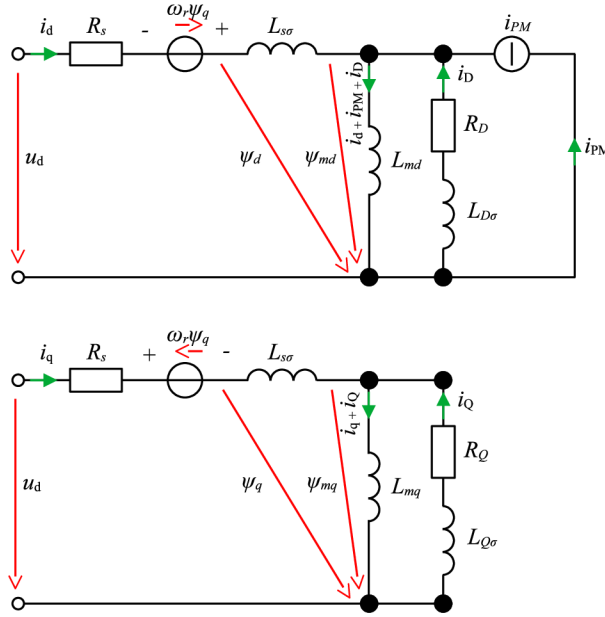


Fig. 1.6: Equivalent circuit of permanent magnet synchronous machine

Equivalent circuit of the both axis shows stator resistance  $R_s$  and stator leakage inductance  $L_{s\sigma}$ . In the d-axis is shown magnetizing inductance  $L_{md}$ , damper resistance  $R_D$  and damper leakage inductance  $L_{D\sigma}$ . The permanent magnet is represented by a current source  $i_{PM}$ . The equivalent circuit in the q-axis shows magnetizing inductance  $L_{mq}$ , damper resistance  $R_Q$  and damper leakage inductance  $L_{Q\sigma}$ .

If the damping winding is included then according to [7]

$$0 = R_Q i_Q + \frac{d\psi_Q}{dt}, \quad (1.3)$$

where  $\psi_Q$  is the damper winding flux linkage in the q-axis.

$$\psi_Q = L_{mq}i_q + L_Qi_Q, \quad (1.4)$$

where  $L_Q$  is total damper inductance in the q-axis and is defined as

$$L_Q = L_{mq} + L_{Q\sigma}. \quad (1.5)$$

In the d-axis are damper winding equations

$$0 = R_D i_D + \frac{d\psi_D}{dt} \quad (1.6)$$

where  $\psi_D$  is damper winding flux linkage that can be calculated as

$$\psi_D = L_{md}i_d + L_Di_D + \psi_{PM}, \quad (1.7)$$

where  $\psi_{PM}$  is permanent magnet flux linkage and  $L_D$  is the total damper inductance in the d-axis and may be calculated as

$$L_D = L_{md} + L_{D\sigma}. \quad (1.8)$$

The virtual current produced by a permanent magnet is

$$i_{PM} = \frac{\psi_{PM}}{L_{md}}. \quad (1.9)$$

The virtual current is not constant because magnetizing inductance  $L_{md}$  depends on the saturation. Stator flux linkage in the q-axis is

$$\psi_q = L_q i_q + L_{mq} i_Q \quad (1.10)$$

The stator flux linkage in the d-axis is

$$\psi_d = L_d i_d + L_{md} i_D + \psi_{PM} \quad (1.11)$$

The product of stator flux linkage in the q-axis and d-axis is the total stator flux linkage

$$\psi_S = \sqrt{\psi_d^2 + \psi_q^2} \quad (1.12)$$

The power factor of a permanent magnet synchronous machine can be written as

$$\cos \varphi = \frac{u_d i_d + u_q i_q}{u_s i_s} \quad (1.13)$$

## 1.2.2 Phasor diagram of PMSM

The phasor diagram of non-salient permanent magnet synchronous machine is same for outer rotor and also for inner rotor machine and is shown in the figure 1.7. This diagram shows example of one phase of machine and it is constructed in pu. Parameters of the machine are:  $\omega_s = 1$  pu,  $u_s = 1$  pu,  $i_s = 1$  pu,  $\psi_s = 1$  pu,  $i_d = 0.24$  pu in the negative direction, that means, the machine is operating in light field weakening. The inductances are  $L_q = L_d = 0.5$  pu, resistance is neglected and rotor position angle is  $\theta_r = 40^\circ$  measured from the x-axis to d-axis, in which  $\psi_{PM}$  is located. The stator reference frame is xy and the rotor reference frame is dq.

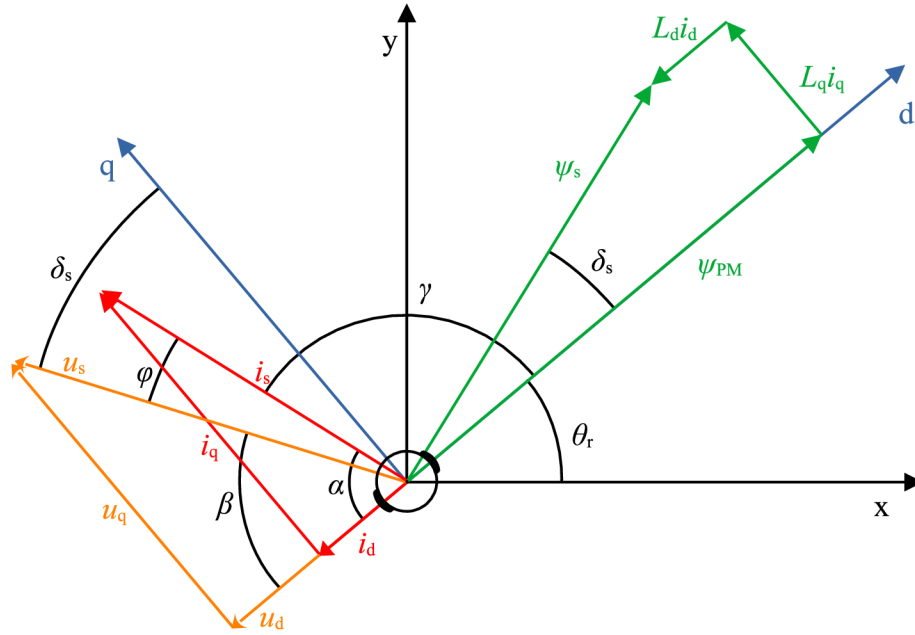


Fig. 1.7: Phase diagram of permanent magnet synchronous machine

In this diagram, the  $\delta_s$  is the load angle, the  $\varphi$  is the angle between current and voltage and is used to power factor calculation  $\cos \varphi$ , and the  $\gamma$  is the current angle measured between d-axis and stator space vector.

The  $\gamma$  angle is beneficial for deriving the machine's torque. This angle can be calculated as

$$\gamma = 90^\circ + \delta_s - \varphi. \quad (1.14)$$

The equation of  $\delta_s$  is

$$\delta_s = \arccos \left( \frac{\psi_s \cos \delta_s}{\psi_s} \right) =, \quad (1.15)$$

where  $\psi_s \cos \delta_s$  is equal to  $\psi_d$  and for its calculation can be used to phasor diagram in the figure 1.7. From this diagram it can be seen, that the equation for  $\psi_d$  is

$$\psi_d = \psi_s \cos \delta_s = \sqrt{\psi_s^2 - (L_q i_q)^2}, \quad (1.16)$$

where

$$i_q = \sqrt{i_s^2 - i_d^2}. \quad (1.17)$$

From the diagram, the  $\varphi$  is

$$\varphi = \alpha - \beta, \quad (1.18)$$

where

$$\alpha = \arccos \frac{i_d}{i_s}. \quad (1.19)$$

The  $\beta$  is also from diagram

$$\beta = 90^\circ - \delta_s. \quad (1.20)$$

### 1.2.3 Torque of PMSM

Synchronous machines generate high torque, that can be according to [7] derived from

$$T_e = \frac{P}{\omega_s}, \quad (1.21)$$

where  $P$  is the power of the machine and can be calculated as

$$P = u_s i_s \cos \varphi. \quad (1.22)$$

The angle  $\varphi$  is equal to  $((\frac{\pi}{2} + \delta_s) - \gamma)$ . Therefore

$$P = u_s i_s \cos \left( \left( \frac{\pi}{2} + \delta_s \right) - \gamma \right). \quad (1.23)$$

Then the next equation can be derived by the goniometric formula  $\sin(x) = \cos \left( x - \frac{\pi}{2} \right)$

$$P = u_s i_s \cos \left( \left( \frac{\pi}{2} + \delta_s \right) - \gamma \right) = u_s i_s \sin (\gamma - \delta_s). \quad (1.24)$$

After using  $\sin(x - y) = \sin(x) \cos(y) - \cos(x) \sin(y)$  the equation can also be written as

$$P = u_s i_s \sin (\gamma - \delta_s) = u_s i_s (\sin \gamma \cos \delta_s - \cos \gamma \sin \delta_s). \quad (1.25)$$

Figure 1.7 reveals that

$$i_d = i_s \cos \gamma, \quad (1.26)$$

$$i_q = i_s \sin \gamma, \quad (1.27)$$

$$u_d = -u_s \sin \delta_s = -\omega_s L_q i_q, \quad (1.28)$$

$$u_q = -u_s \cos \delta_s = \omega_s (\psi_{PM} + L_d i_d). \quad (1.29)$$

By using equations 1.26- 1.29 the pu power factor can be expressed as

$$P = \omega_s \left[ \psi_{PM} i_s \sin \gamma - i_s^2 \sin 2\gamma \left( \frac{L_q - L_d}{2} \right) \right]. \quad (1.30)$$

The final torque formula is

$$T_e = \frac{P}{\omega_s} = \psi_{PM} i_s \sin \gamma - i_s^2 \sin 2\gamma \left( \frac{L_q - L_d}{2} \right). \quad (1.31)$$

## 2 Losses in permanent magnet synchronous machine

This chapter is focused on all types of losses generated in permanent magnet synchronous machines. The two most important types of the losses are iron and copper losses. The copper losses become dominant when the machine is loaded; usually, on the other hand, the magnetic losses are dominant when the machine is in the no-load condition. The mechanical losses are normally a minor part of total losses. Only in the case of the high-speed machines are dominant. [9]

If the PWM is used to supply the permanent magnet synchronous machine, then according to [9] the PWM losses can not be neglected. These losses might represent almost one-third of total stator no-load magnetic losses.

Separation, accurate evaluation, and region of the loss excitation are essential parts of the thermal analysis. It is because all losses generate heat in the parts of the machine where they are generated. The individual types of machine losses are shown in the figure 2.1.

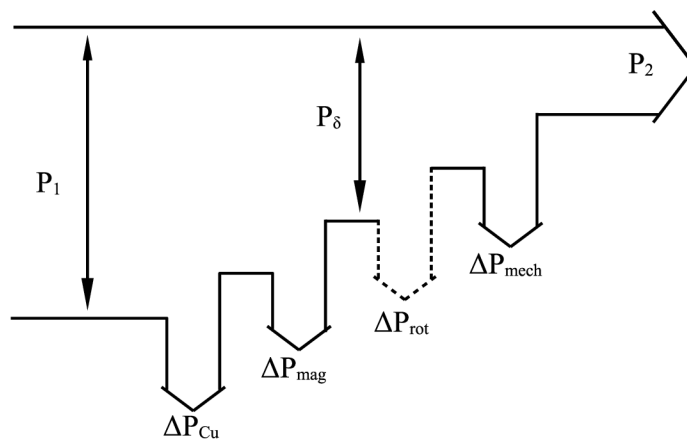


Fig. 2.1: Machine loss dividing

Total losses generated in machines can be defined as a summary of partial losses. That means total losses might be calculated as

$$\Delta P_{\text{tot}} = \Delta P_{\text{Cu}} + \Delta P_{\text{mag}} + \Delta P_{\text{rot}} + \Delta P_{\text{mech}}, \quad (2.1)$$

where  $\Delta P_{\text{Cu}}$  are stator copper losses,  $\Delta P_{\text{mag}}$  are stator magnetic losses,  $\Delta P_{\text{rot}}$  are rotor losses and  $\Delta P_{\text{mech}}$  are mechanical losses.

## 2.1 Stator copper losses

Stator copper losses are losses generated in the stator winding. The winding is an significant source of loss in the electrical machine. In the [8] are presented that copper losses in the three-phase machine can be calculated as

$$\Delta P_{\text{Cu}} = 3R_{\text{ph}}I_{\text{ph}}^2, \quad (2.2)$$

where  $R_{\text{ph}}$  is the DC resistance of each phase and  $I_{\text{ph}}$  is the phase current. The accuracy calculation of this loss type looks very simple at first sight, but it is not. It is because the DC resistance  $R_{\text{ph}}$  is temperature-dependent, which means with increasing temperature, this resistance increases too. Changing this resistance is according to [8] defined by

$$R_{\text{ph},n} = R_{\text{ph},0} (1 + \alpha_{\text{Cu}}\Delta T), \quad (2.3)$$

where  $R_{\text{ph},n}$  is the new phase resistance,  $R_{\text{ph},0}$  is the phase resistance at the reference temperature (usually it is 20 °C),  $\alpha_{\text{Cu}}$  is the temperature coefficient of resistance ( $\approx 0.0042 \text{ K}^{-1}$ ) and  $\Delta T$  is  $(T_{\text{ph},n} - T_{\text{ph},0})$ .

This temperature dependence of resistance proves how much the thermal and electromagnetic analyses depend on each other and how necessary the use of cooling is in the machines. However, this is not the only factor affecting the machine's copper losses. In the [9] have been described two more effects that influence losses in the stator winding. These two effects are the skin effect and proximity effect. The skin effect arises due to eddy currents generated in the center of the conductor. The proximity effect is a similar phenomenon but created by the current flow in other conductors in the same slot.

Both proximity effect and skin effect influence the distribution of the current densities in the conductors of winding. That means both effects can change the AC resistance of the wires and the corresponding losses in high-frequency electrical machines. These effects might be reduced by dividing conductors into electrically isolated parallel smaller ones.

## 2.2 Stator magnetic losses

In this section, the separation of magnetic losses into different losses types is described. These types are hysteresis, eddy current, and excess losses. The separation of iron losses into these types simplifies this complex physical phenomenon. Total stator magnetic losses are the result of a summary of these separated parts.

$$\Delta P_{\text{mag}} = \Delta P_{\text{hys}} + \Delta P_{\text{eddy}} + \Delta P_{\text{ex}}, \quad (2.4)$$



where  $\Delta P_{\text{hys}}$  are hysteresis losses,  $\Delta P_{\text{eddy}}$  are eddy current losses and  $\Delta P_{\text{ex}}$  are excess losses.

### 2.2.1 Hysteresis losses

According to [9] the hysteresis losses in homogenous material with purely sinusoidal excitation can be calculated as

$$\Delta P_{\text{hys}} = k_{\text{h}} f B_{\text{m}}^{\alpha}, \quad (2.5)$$

where  $k_{\text{h}}$  is experimental coefficient,  $f$  is frequency,  $B_{\text{m}}$  is amplitude of the flux density and  $\alpha$  is experimental coefficient.

A combination of used experimental coefficients in (2.5) makes the accuracy of calculation worse in the whole range of flux densities. More accurate results are the reason why [10] apply different coefficients for each range.

### 2.2.2 Eddy current losses in a laminated material

Several methods might analyze eddy current losses in laminated material. These methods are analytical or based on FE (Finite element method), and the losses might be calculated directly or in the post-processing. In this thesis, some of these methods are described.

The analytical method calculation is according [11]

$$\Delta P_{\text{eddy}} = k_{\text{e}} f^2 B_{\text{m}}^2, \quad (2.6)$$

where  $k_{\text{e}}$  is eddy current coefficient. The  $k_{\text{e}}$  is according to [11] defined as

$$k_{\text{e}} = \frac{\pi^2 d^2 V}{6\rho}, \quad (2.7)$$

where  $\rho$  is the resistivity of the material and  $d$  is thickness of lamination.

One of the 2D-FE methods is an estimation of eddy current losses in the time domain which is usually used in the post-processing stage. Evaluation of eddy current losses by this method is based on the equation

$$\Delta P_{\text{eddy}} = \frac{1}{T} \frac{d^2}{12\rho} \int_0^T \left| \frac{dB}{dt} \right|^2 dt, \quad (2.8)$$

where  $T$  is period, and  $B$  is flux density. This equation does not consider the orthogonal components of flux density, but the final flux density vector consists of two orthogonal components that can be defined as

$$\vec{B} = B_{\text{x}}\vec{x} + B_{\text{y}}\vec{y}, \quad (2.9)$$

where  $B_x$  is x-axis flux density component,  $\vec{x}$  is unit vector,  $B_y$  is y-axis flux density component and  $\vec{y}$  is unit vector. After time derivation amplification of the absolute value of equation 2.9 can be written as

$$|\dot{B}|^2 = |\dot{B}_x^2 + \dot{B}_y^2|. \quad (2.10)$$

This equation proves that total eddy current losses are equal to the sum of eddy current losses due to their orthogonal components.

It is described in [12] that finite element software gives the flux density data within the Cartesian plane. The components of the flux density can be calculated as

$$\begin{pmatrix} B_r \\ B_\theta \end{pmatrix} = \begin{pmatrix} \cos(\theta) & \sin(\theta) \\ -\sin(\theta) & \cos(\theta) \end{pmatrix} \begin{pmatrix} B_x \\ B_y \end{pmatrix}, \quad (2.11)$$

where  $B_r$  is radial component of flux density,  $B_\theta$  is peripheral component of flux density  $\theta$  is angel between the  $B_r$  vector and positive x-axis in the xy plane. Total eddy current losses in the iron volume, in the discrete-time domain and taking into account components of the flux density are according to [13], [10] defined as

$$\Delta P_{\text{eddy,tot}} = k_{\text{ed}} \frac{d^2}{12\rho} \int_{\text{Fe}} \frac{1}{N_p} \sum_{k=2}^{N_p} \left\{ \left( \frac{B_r^{k+1} - B_r^k}{\Delta t} \right)^2 + \left( \frac{B_\theta^{k+1} - B_\theta^k}{\Delta t} \right)^2 \right\} dv, \quad (2.12)$$

where  $k_{\text{ed}}$  is eddy current loss coefficients, the  $N_p$  is the number of time steps per period.

### 2.2.3 Excess losses

Excess losses represent the non-uniform distribution of magnetization across the lamination. The ratio of non-uniform distribution depends on the presence, orientation, and size of the magnetic domains. Every domain does not have the same orientation, which makes the concentration of eddy currents higher. The larger size of the magnetic domains also negatively influences the excess losses. [14], [9]

The excess losses are according to [9] defined as

$$\Delta P_{\text{ex}} = k_{\text{ex}} (f B_m)^{\frac{3}{2}}, \quad (2.13)$$

where  $k_{\text{ex}}$  is the coefficient determined by curve fitting for the used material.

## 2.3 Rotor losses

In permanent magnet synchronous machines, the rotor losses are produced by slot harmonics, time harmonics, and space harmonics. The rotor losses reduce the efficiency of the machine and increase its temperature. The too high temperature of

the rotor might bring demagnetization of permanent magnets used in this machine type.

If the permanent magnet synchronous machine is well designed, the rotor losses are, according to [7] insignificant and do not affect the efficiency. That means the rotor losses might be neglected in this type of machines.

## 2.4 Mechanical losses

Mechanical losses in permanent magnet synchronous machines consist of bearing friction losses and gas friction losses. These two parts of mechanical losses are described below.

### 2.4.1 Bearing losses

Bearing losses might be calculated by tools provided by the manufacturer or by applying empirical formulas. According to [15] the formula usable for mechanical losses is

$$P_b = 0.5C_{fb}Fd_b\omega, \quad (2.14)$$

where  $C_{fb}$  is the contact coefficient of friction,  $F$  is the equivalent dynamic bearing load,  $d_b$  is bearing bore diameter and  $\omega$  is the angular frequency of the shaft. The  $F$  can be calculated from the radial and axial components of the bearing load.

Another way of calculating bearing mechanical losses is according [16]

$$P_b = 0.06k_{fb}m_r\frac{n}{60}, \quad (2.15)$$

where  $k_{fb}$  is equal to  $1\div 3 \text{ m}^2/\text{s}^2$  and its value depends on the bearing specifications,  $m_r$  is the mass of the rotor and  $n$  is the speed of rotor.

### 2.4.2 Gas frictional losses

The product of rotor movement and gas flow in the machine is the gas friction losses. In the figure 2.2 are shown, all free types of flow. These types are according to [17]:

- Tangential flow generates by rotation of the rotor
- Axial flow generates the flow of cooling gas through the air gap
- Taylor vortices, due to centrifugal forces

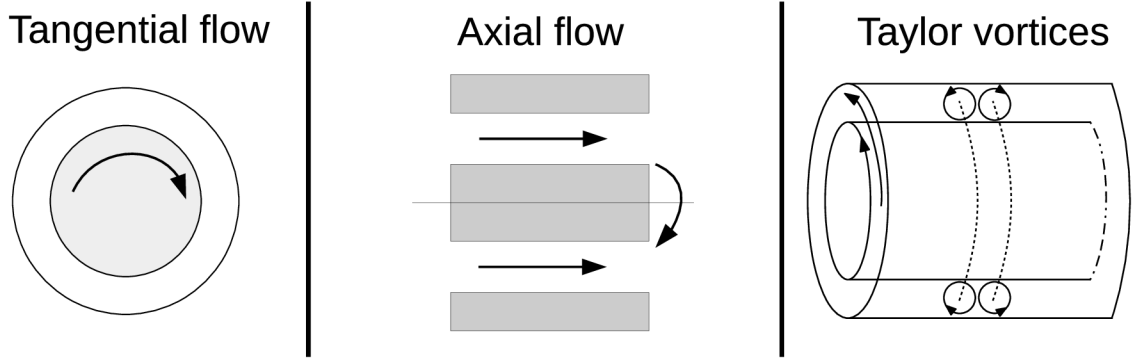


Fig. 2.2: Flow origins

Moreover, the fluid flow in the machine might be divided into laminar and turbulent. This division is based on the ratio of inertia and viscous forces.

The power losses due to gas friction in the air gap of the rotating rotor, which is modeled as a rotating cylinder, can be according [7] expressed as

$$\Delta P_{\rho,1} = \frac{1}{16} k_{ro} C_{f,1} \pi \rho \omega^3 D_{s,in}^4 L, \quad (2.16)$$

where  $k_{ro}$  is roughness coefficient of material (for smooth material is equal to 1),  $C_{f,1}$  is the friction coefficient,  $\rho$  is the density of the coolant,  $D_{s,in}$  is the outer diameter of air gap, and  $L$  is the rotor length.

The turbulence indicator in the air gap is the Couette Reynolds number. This number is according to [17]

$$Re_{\delta} = \frac{\rho \omega D_{s,in} \delta}{2\mu}, \quad (2.17)$$

where  $\delta$  is the air gap thickness and  $\mu$  is the dynamic viscosity of the coolant.

The friction coefficient is the function of Couette Reynolds number and according to [7] is expressed as

$$\begin{aligned} C_{f,1} &= \frac{\left(\frac{\delta}{r}\right)^{0,3}}{Re_{\delta}^{0,6}} && \text{pro } Re_{\delta} < 64, \\ C_{f,1} &= 5 \frac{\left(\frac{\delta}{r}\right)^{0,3}}{Re_{\delta}} && \text{pro } 64 < Re_{\delta} < 500, \\ C_{f,1} &= 0,515 \frac{\left(\frac{\delta}{r}\right)^{0,3}}{Re_{\delta}^{0,5}} && \text{pro } 500 < Re_{\delta} < 10^4, \\ C_{f,1} &= 0,0325 \frac{\left(\frac{\delta}{r}\right)^{0,3}}{Re_{\delta}^{0,2}} && \text{pro } Re_{\delta} > 10^4. \end{aligned} \quad (2.18)$$

The power losses generated by rotor end rings can be according to [17] expressed as

$$\Delta P_{\rho,2} = \frac{1}{64} C_{f,2} \pi \rho \omega^3 (D_{s,in}^5 - D_r^5), \quad (2.19)$$

where  $C_{f,2}$  is the friction coefficient and  $D_r$  is the rotor diameter.

In the case of the end rings region, the Couette Reynold number can, according to [17] be calculated as

$$\text{Re}_r = \frac{\rho\omega D_{s,\text{in}}^2}{4\mu}. \quad (2.20)$$

The friction coefficient is according to [17] is defined as

$$\begin{aligned} C_{f,2} &= \frac{3,87}{\text{Re}_r^{0,5}} \quad \text{for } \text{Re}_r < 3 \cdot 10^5, \\ C_{f,2} &= \frac{0,146}{\text{Re}_r^{0,2}} \quad \text{for } \text{Re}_r > 3 \cdot 10^5. \end{aligned} \quad (2.21)$$

## 3 Heat transfer

Thermal analysis is a crucial part of electrical machine design. Three mechanisms of heat transfer (convection, conduction, and radiation) are described in this section. These methods describe thermal transfer from warmer regions to the cooler regions of the machine.

### 3.1 Conduction

In solid materials, conduction is the major mechanism of heat transfer, this mechanism is also in the fluid materials, but the quantity of transferred heat is minor. That means that the conductive heat transfer is insignificant in the fluid materials and can be neglected.

Thanks to the high thermal conductivity of metal materials extensively used in electrical rotating machines, the mechanism of conduction is very extended. The quantity of transferred heat depends on the geometry and properties of the material. The transferred heat can be according to [18] expressed as

$$Q_{\text{cond}} = \lambda S \frac{T_1 - T_2}{d}, \quad (3.1)$$

where  $\lambda$  is thermal conductivity,  $T_1$  is the temperature on the one side of a solid, and  $T_2$  is the temperature on the second side of the solid and  $d$  is thickness of the solid. The difference in temperatures can be written as

$$\Delta T = T_1 - T_2. \quad (3.2)$$

Heat flux through the simple plane wall, which is shown in the figure 3.1 is according to [19], [20]

$$q = QS, \quad (3.3)$$

where the  $q$  is heat flux which is defined as

$$q = \frac{\lambda \Delta T}{d}. \quad (3.4)$$

The thermal resistance of a single plane wall can be expressed as

$$R_T = \frac{\Delta T}{Q}. \quad (3.5)$$

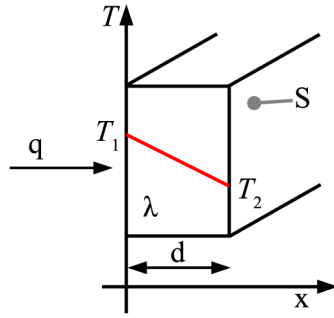


Fig. 3.1: Heat transfer through the plane wall

The situation of heat transfer through the cylindrical wall in the radial direction is shown in the figure 3.2. Heat flow through the simple cylinder in the radial direction is in the [21] defined as

$$Q = \frac{2\pi L \Delta T}{\frac{1}{\lambda} \ln \frac{r_2}{r_1}}, \quad (3.6)$$

where  $L$  is the length of a cylinder,  $r_1$  is the inner radius of the cylinder, and  $r_2$  is the outer radius of the cylinder. The thermal resistance of the cylinder in the radial direction can be calculated as

$$R_{\text{cond,cyl}} = \frac{\ln \left( \frac{r_2}{r_1} \right)}{2\pi \lambda L}. \quad (3.7)$$

The thermal resistance of a solid bar in the radial direction is defined as

$$R_{\text{cond,bar}} = \frac{1}{8\pi \lambda L}. \quad (3.8)$$

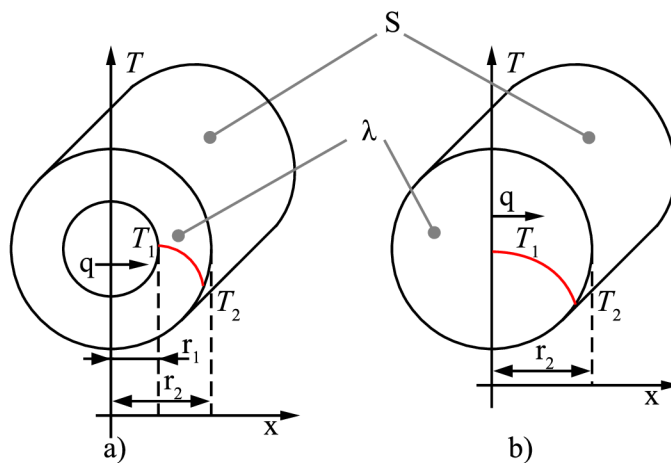


Fig. 3.2: Heat transfer in the cylinder and cylindrical bar

## 3.2 Convection

Convection is the main mechanism of heat transfer in fluid materials. This mechanism helps transfer heat from solid bodies into the ambient fluid. The primary condition of effective cooling by the fluid is the movement of that fluid. If the fluid is static, there is only conduction heat transfer in it. However, fluids do not have good conduction. [18]

According to [18] there are two types of heat transfer by convection in the fluids. These types are natural convection and forced convection, and they are described in this section. Heat flow of convection heat transfer is according to [18] defined by the formula

$$Q_{\text{conv}} = hS\Delta T, \quad (3.9)$$

where  $h$  is the heat transfer coefficient. This coefficient can be according to [22] defined as

$$h = \frac{N_u \lambda}{L_c}, \quad (3.10)$$

where  $L_c$  is the characteristic length and  $N_u$  is the Nusselt number.

The Nusselt number tells how much better is heat transfer of moving fluid than heat transfer of static fluid. That means a higher value of this number describes the higher heat transfer efficiency. If the Nusselt number is equals to 1 only conduction heat transfer takes place. That means the fluid is still.

The convection thermal resistance is according to [20] defined as

$$R_{\text{conv}} = \frac{1}{hS}. \quad (3.11)$$

### 3.2.1 Natural convection

This type of convection is characterized by spontaneous generation of it. This spontaneous flow is a consequence of temperature differences through single parts of the fluid [19]. In electrical machines, natural convection takes place only in very few cases. Usually, it is considered only during the cooling of the machine's frame into the ambient fluid.

Visualization of the natural convection is shown in the figure 3.3. The principle of natural convection is that cold air flows downwards. There the warm solid heating up this cold fluid. This fluid cools down the solid and heats itself. Then the warmed fluid rises. If this solid is placed in some closed container, the vortex is generated there. [18]



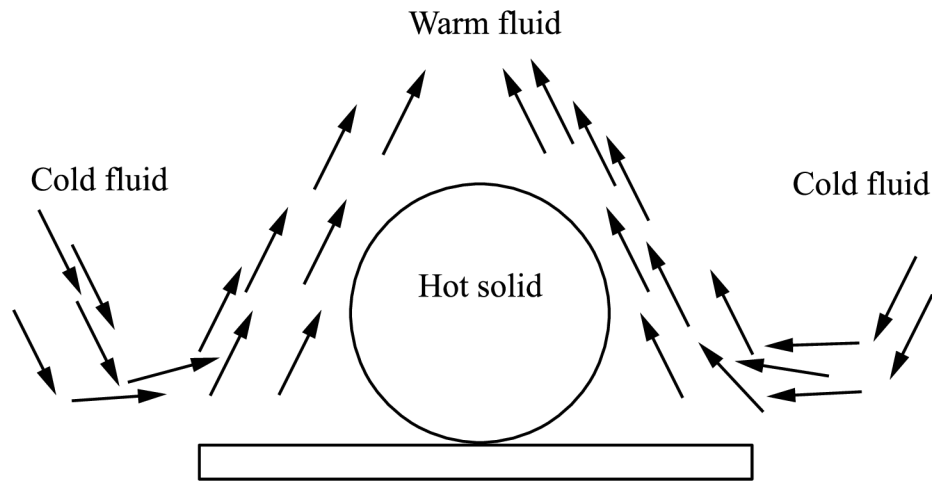


Fig. 3.3: Natural convection

### 3.2.2 Forced convection

External forces generate forced convection. Its advantage is the much better cooling efficiency. This type of convection is usually used in electrical rotating machines. [18]. In electrical machines, it is always used in the inner parts of machines.

The example of generation of the forced flow is shown in the figure 3.4. The fan blows the cold fluid towards the hot solid. This hot solid is cooled into the fluid and heats it. The warmer fluid continues in the same direction as the cooled fluid before heating. This type of convection is more efficient than natural convection.

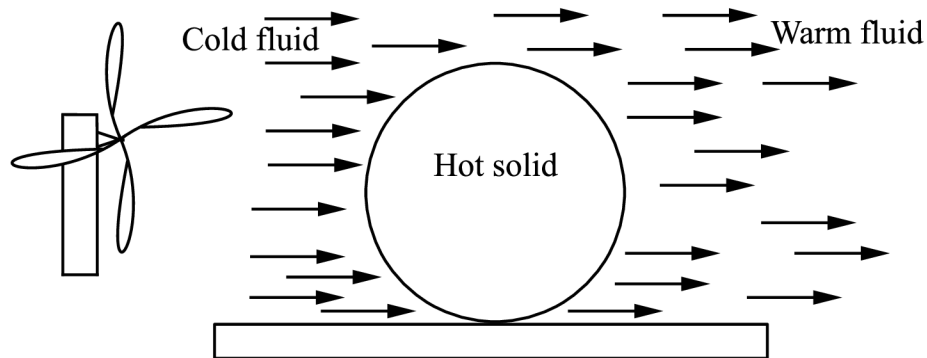


Fig. 3.4: Forced convection

## 3.3 Radiation

The radiation transfer of heat is based on electromagnetic radiation. Solids around temperatures about 500-560 °C generate radiation in the infrared part of the electromagnetic spectrum, and solids with higher temperatures generate radiation in the

visibility part of the spectrum. Every solid with a higher temperature than absolute zero generates the radiation. [19], [21]

Because the radiation heat transfer is based on electromagnetic radiation, it does not need any medium. That means every solid can emit and absorb heat through radiation. An overall radiation flow of solid is according to [19] defined as

$$\phi = \phi_r + \phi_{tr} + \phi_a, \quad (3.12)$$

where  $\phi_r$  is the reflected part of flux,  $\phi_{tr}$  is the transmitted part of flux and  $\phi_a$  is the absorbed part of flux. It is essential to know the quantity of the radiation in electrical machines so the heat flow can be according [18] derivated as

$$Q_{\text{rad}} = \varepsilon \sigma S T^4, \quad (3.13)$$

where  $\varepsilon \in < 0; 1 >$  is the emissivity of the solid surface,  $\sigma = 5.67 \cdot 10^{-8} \text{W} \cdot \text{m}^{-2} \cdot \text{K}^{-4}$  is Stefan-Boltzmann constant and  $T$  is the thermodynamic temperature of the surface. In the case where one solid is completely enclosed in the other solid the heat flux is defined as

$$Q_{\text{rad}} = \varepsilon \sigma S (T_1^4 - T_2^4), \quad (3.14)$$

where  $T_1$  is the thermodynamic temperature of the inner solid and  $T_2$  is the thermodynamic temperature of the outer solid. [21]

### 3.4 Machine cooling

According to [28] the heat generated in the electrical machine must be transferred from it to the air, water, or the earth. This heat transfer can be done in several ways.

One of the ways capable of using to cool machines is the direct cooling. This system can be made by circulating the coolant medium over the hot surface. This medium transmits the thermal energy from the surface into the ambient. In electrical rotating machines, the direct cooling system in the air is the most commonly used. [28]

Another way of cooling is using an indirect system of cooling. This system uses two circuits of cooling. The first circuit uses fluid types as air, oil, or water to remove heat from the heated surface to the outside, where the second circuit is situated. The second circuit uses water or air, which removes the heat from the first circuit and transmits it into the ambient. [28]

The permanent magnet synchronous machines with an outer rotor usually use the same system as machines with inner rotor machines, which is a direct system of cooling based on the air. The air is commonly used because of its high mobility,

which is very useful in rotating machines. The rotor is directly cooled into the ambient. The cooling effect of machines with outer rotor increase thanks to the large air gap between the bell and mounting flange. The heat from stator is removed through several paths. One of these paths is through the bearing, shaft, and mounting flange into the ambient. The second path is from the stator to the air gap between the mounting flange and stator packet. And another path is from the stator through the inner air, permanent magnet, rotor bell into the ambient. [28], [23] The thermal resistance of the second path is defined by equation (3.18). The described paths of heat removing from stator are shown in the picture 5.3. These ways are between node  $T_s$  and  $T_{amb}$ .

The thermal analysis in electrical rotating machines might be performed in several ways. One of these ways is the method of thermal network. The principle of this method is dividing the machine into basic thermal elements that represent a combination of heat transfer mechanisms which are described in section 3. [25]

The computing time of the thermal network method is much less than that of the finite element method. This short computing time makes it suitable for real-time modeling of machine temperatures. Moreover, reducing the complexity of the thermal model into several necessary nodes has a positive influence on computing time and complexity. [26] On the other hand, reducing network nodes brings greater demands on engineering knowledge.

Many nodes and thermal resistances are defined in the field of the unreduced thermal network. However, these resistances are more simple and have been defined early as the equations (3.5),(3.7),(3.8),(3.11).

Nevertheless, reducing the number of thermal network nodes brings more complex formulas for thermal resistances, but less resistance calculation is needed. An example of several resistances replaced by one is equation

$$R_{cond} = \frac{1}{2\pi\lambda L_s p_{ir}} \ln\left(\frac{d_2}{d_1}\right), \quad (3.15)$$

where  $L_s$  is stator length and  $p_{ir}$  is the ratio between stator teeth iron volume and the total volume of stator iron. This equation is defined by [4] and combines the resistances of teeth and stator yoke into one. Nevertheless, reducing the number of thermal network nodes brings more complex formulas for thermal resistances, but less partial calculations of them are needed.

### 3.5 Modelling of speed-dependent resistances

A very complex part of the analysis is analyzing the thermal resistance of the cooling path from the winding system and stator lamination through the air gap between

the rotor bell and the mounting flange into the ambient air. This thermal resistance can according to [23] decrease based on the machine speed. The decreasing might be approximating either linear 3.16 or quadratic 3.18.

If the linear decreasing of the speed dependency thermal resistance is considered, the thermal resistance is defined as

$$R_{\text{lin},i}(n) = R_{i,0} \left( 1 - \frac{|n|}{n_{\text{max}}} (1 - k_{i,s}) \right) + \Delta R_{i,0} \delta(n), \quad (3.16)$$

where  $n$  is the speed of rotor bell,  $R_{i,0} = R_i(0)$  is the additional thermal resistance at zero speed,  $n_{\text{max}}$  is the maximum speed of the rotor bell,  $k_{i,s}$  is the parameter to be optimized and its value is equal to  $0 \div 1$ . The  $\delta(n)$  is the delta distribution  $\Delta R_{i,0}$  is value of thermal resistance by which  $R_{i,0}$  is increased at zero speed of machine. The delta distribution is according to [24] defined as

$$\delta(n) = \begin{cases} 1, & \text{if } n = 0 \\ 0, & \text{if } n \neq 0 \end{cases}. \quad (3.17)$$

The quadratic waveform of the thermal resistance dependent on the equation

$$R_{\text{quad},i}(n) = R_{i,0} \left( k_{i,s} + \left( \frac{|n|}{n_{\text{max}}} - 1 \right)^2 (1 - k_{i,s}) \right) + \Delta R_{i,0} \delta(n). \quad (3.18)$$

Both, linear and quadratic waveforms are observed in the part a) in the figure 3.5. The part b) observed the detail of red waveform showed in the same picture.

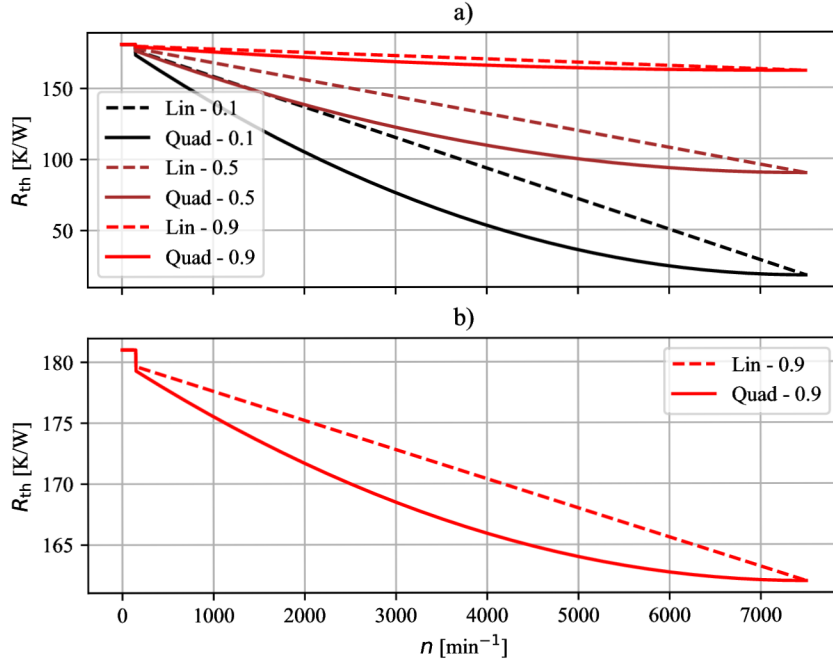


Fig. 3.5: Linear and quadratic conduction heat resistances

From the picture, it can be seen that the parameter  $k_{i,s}$  affects the rate of change of the thermal resistance waveform. A lower parameter value increases the rate of change, and a higher value decreases the rate of change.

Another way of speed-dependent thermal resistance analysis is through the (3.11) where the heat transfer coefficient calculation is considered directly. There are several ways how to model speed dependence of heat transfer coefficient. One of these ways is according to [27] defined as a

$$h = c_1 (1 + c_2 \nu^{c_3}), \quad (3.19)$$

where  $c_1$ ,  $c_2$  and  $c_3$  are coefficients that are described in the [27] and  $\nu$  is inner air speed. In the field of electrical machines are rotates per minute usually considered so the  $\nu$  can be calculated as

$$\nu = \frac{2\pi n}{60} r, \quad (3.20)$$

$r$  is the inner radius of rotor. This formula defines the speed of the rotor, but in the context of simplification, is the speed of inner air considered the same.

Influence of individual coefficients to resulting waveform is shown in the picture 3.6. This graph shows that  $c_1$  sets the initial value of the heat transfer coefficient waveform. The  $c_2$  defines the steepness of the waveform, and the  $c_3$  defines if the heat transfer coefficient function is convex, linear, or concave.

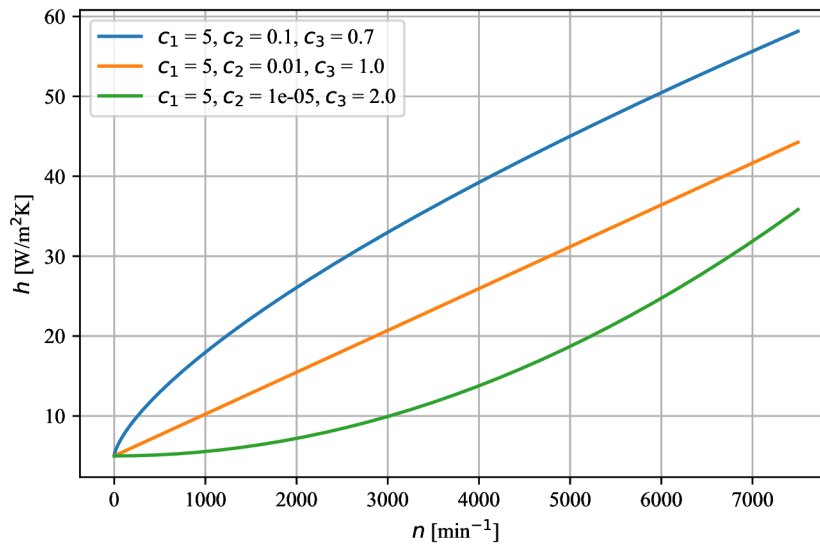


Fig. 3.6: Heat transfer coefficient different  $c_1$ ,  $c_2$  and  $c_3$

### 3.5.1 Heat transfer coefficient derivation

This chapter describe another ways of heat transfer coefficient approximation. These approximations are based on the resistances (3.16) and (3.18).

First, the derivation of heat transfer coefficient approximation based on the (3.16) is described. This heat transfer coefficient is called linear in this thesis because it is based on linear dependency of convection thermal resistance. So the derivation is based on the substitution of the  $R_{\text{lin},i(n)}$  by the  $\frac{1}{h_i S}$  and the result of this substitution is

$$\frac{1}{h_i S} = R_{i,0} \left( 1 - \frac{|n|}{n_{\text{max}}} (1 - k_{i,s}) \right). \quad (3.21)$$

Then the formula can be modified as

$$h_i = \frac{1}{SR_{i,0} \left( 1 - \frac{|n|}{n_{\text{max}}} (1 - k_{i,s}) \right)}, \quad (3.22)$$

where  $SR_{i,0}$  can be substituted by  $\frac{1}{h_0}$ . The final result of the linear speed-dependency for the  $h_i$  is

$$h_i = h_0 \frac{n_{\text{max}}}{n_{\text{max}} - n(1 - k_{i,s})}. \quad (3.23)$$

where  $h_0$  is initial value of heat transfer coefficient. Moreover it is necessary to consider static heat transfer coefficient. This coefficient derivation is based on the considering zero speed of machine in the (3.16).

$$h_{\text{stat}} = \frac{(h_0 \cdot h_\delta)}{(h_0 + h_\delta)} \delta(n), \quad (3.24)$$

where  $h_\delta$  is value of heat transfer coefficient if the rotor does not move. After combining equation (3.22) with equation (3.24) the final formula defines linear approximation of heat transfer coefficient

$$h_{\text{lin}} = h_0 \frac{n_{\text{max}}}{n_{\text{max}} - |n|(1 - k_{i,s})} + \frac{(h_0 \cdot h_\delta)}{(h_0 + h_\delta)} \delta(n). \quad (3.25)$$

Second, the derivation of the heat transfer coefficient based on the equation (3.18) is described lower. This heat transfer coefficient is based on the quadratic dependency of convection thermal resistance, so it is called the quadratic heat transfer coefficient in this thesis. There the  $R_{\text{quad},i(n)}$  is again substituted by the  $\frac{1}{h_q S}$ . Thanks to the substitution the following equation is defined as

$$\frac{1}{h_q S} = \frac{1}{SR_{i,0} \left( k_{i,s} + \frac{|n|}{n_{\text{max}}} - 1 \right)^2 (1 - k_{i,s})}. \quad (3.26)$$

This equation is combined with equation (3.24) and the final formula of quadratic heat transfer coefficient approximation is defined as

$$h_{\text{quad}} = \frac{h_0}{\left( n_{\text{max}} + \left( \frac{|n|}{n_{\text{max}}} \right) - 1 \right)^2 (1 - k_{i,s})} + \frac{(h_0 \cdot h_\delta)}{(h_0 + h_\delta)} \delta(n). \quad (3.27)$$

Both, linear and quadratic approximation of  $h$  are shown in the picture (3.7) a). This picture shows that the lower value of the parameter  $k_{i,s}$  increases rate of the value of the heat transfer coefficient change in this case. There is also shown that the lower value of the  $k_{i,s}$  decrease the rate of heat transfer coefficient change and also makes deviation from the linear and quadratic waveform of it.

The detail of the red waveform is observed in the part b) of the same picture. There are shown waveforms for the  $k_{i,s} = 0.9$  in this part. It shown if the  $k_{i,s} < 0.9$  the approximation of the heat transfer coefficient based on the equation (3.16) looks like it increase exponential. In the case of heat transfer coefficient approximation based on the equation (3.18) the waveform also does not look like a quadratic curve. This parameter causes these deviations in the waveforms.

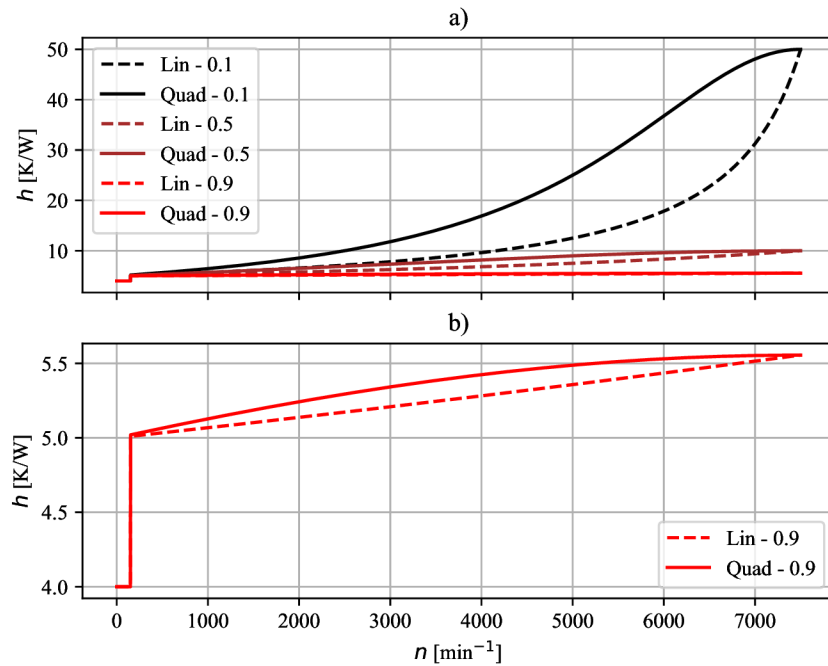


Fig. 3.7: Linear and quadratic heat transfer coefficients approximation

In the picture 3.8 the thermal resistances are calculated through the formula (3.11). In the part a) of this picture the  $h$  with different coefficients and constant  $S$  is considered. These parameters are used in the formula (3.19). On the other hand in the part b) same formula but with constant coefficients and different  $S$  is used. The coefficients considered in this case are  $c_1 = 5$ ,  $c_2 = 5 \cdot 10^{-2}$  and  $c_3 = 0.8$ .

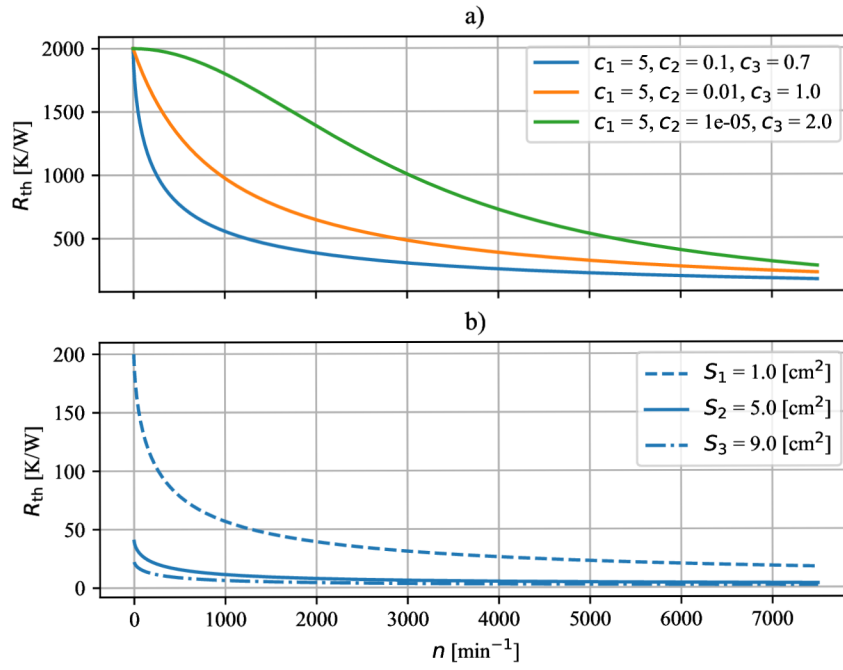


Fig. 3.8: Thermal resistances different  $c_1, c_2, c_3$  and  $S$

In the picture 3.9 the waveform of heat transfer coefficient based on the linear and quadratic heat transfer coefficients are shown.

In the part a) of the picture 3.9 the considered values of the used variables are shown in the table 3.1. In the part b) of the same picture the detail of the red waveform from the case a) is shown.

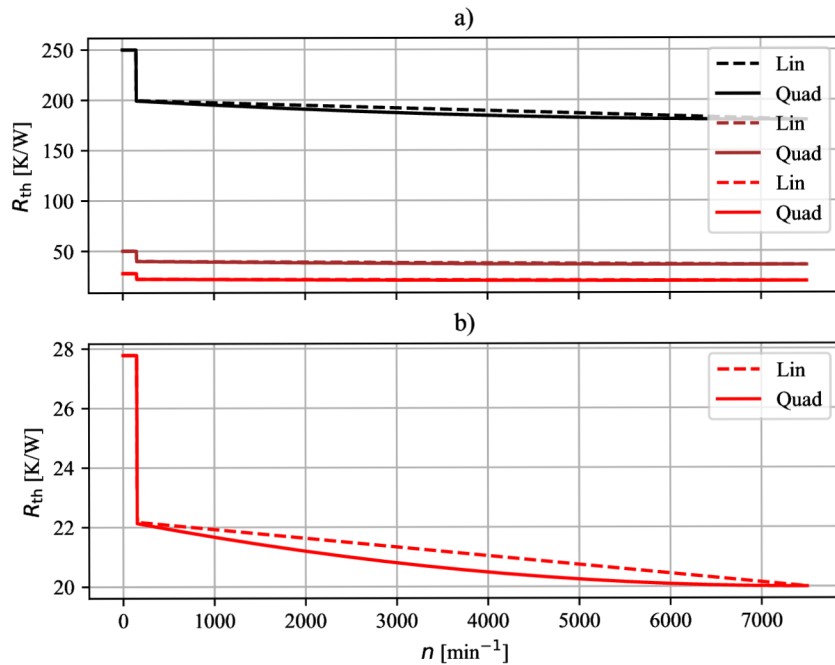


Fig. 3.9: Linear and quadratic thermal resistances



Tab. 3.1: Table of variables used in equations (3.25) and (3.27)

Parameter	Value	Unity
Initial heat transfer coefficient - $h_0$	5	[W/m <sup>2</sup> K]
Static heat transfer coefficient - $h_\delta$	20	
Parameter to be optimized - $k_{i,s}$	0.9	[-]
Heat transfer surface 1 - $S_1$	1	[cm <sup>2</sup> ]
Heat transfer surface 2 - $S_2$	5	
Heat transfer surface 3 - $S_3$	9	

## 4 Optimizing methods

Nowadays, there is continuing demand for automation and mechanization in industry. That means more electrical machines are needed. More electrical machines need much electric power, so higher demand is placed on these machines' efficiency, price, and control. The result of these requirements is the need to better estimate temperatures and optimize single machines for individual applications. [29],[30]

There are described several ways of optimizing the parameters of the thermal network and estimating the machine temperatures in this chapter. The resulting temperatures calculated based on the optimized values are compared with measured temperatures in the chapter 7.1. It is possible to compare which optimizing method is better for optimizing the thermal network parameters thanks to the measured data. The better means which method is, for example, more accurate, need lower computing time and lower computing power.

### 4.1 Genetic algorithm

The genetic algorithm is a method for solving both constrained and unconstrained problems, and it is part of the group named evolutionary algorithms. This method is based on the ideas of natural selection and genetics, which is the process that drives biological evolution. The genetic algorithm is used to compute the high-quality and optimal solutions. [31], [32] The disadvantage of this method is the high computing time and the need for high computing power. The LPTN used for the genetic algorithm is shown in the picture 5.3.

The algorithm simulates the natural selection process, so the individuals from the direct generation are chosen to be parents at each step. These parents are used to produce the children for the next generation. These children represent points in the search area. Children with the better search parameters become the new parents, and the algorithm repeats. [31], [32]

There are three rules of the new population created by this method. [32] These rules are described lower in this section.

#### 4.1.1 Selection rules

There are selected random parents to contribute to the selection of the next generation. The selection of the parents can depend on the individual score. [32] The schematic of the selection principle is shown in the picture 4.1. This picture is inspired by [32] and [31].

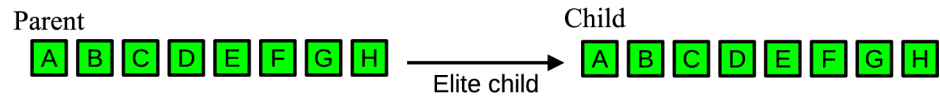


Fig. 4.1: Selection rules

### 4.1.2 Crossover rules

These rules create a new generation by randomly combining two parents. After the combination, a completely new individual is created. [32] There is observed the block diagram of the crossover rules in the picture 4.2. This picture is inspired by [32] and [31].

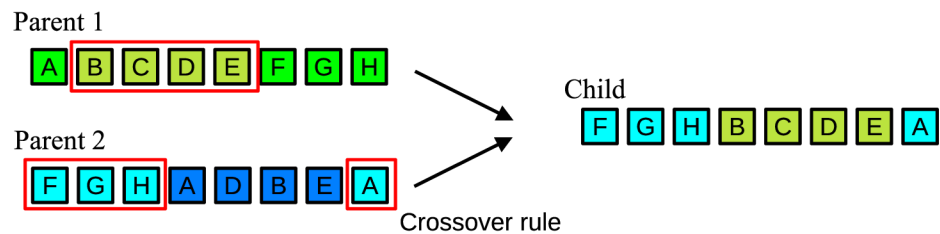


Fig. 4.2: Crossover rules

### 4.1.3 Mutation rules

The mutation creates the new child by applying the random changes to parent's genes [32]. The principle of mutation is shown in the picture 4.3. This picture is inspired by [32] and [31].

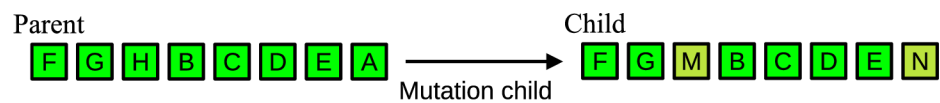


Fig. 4.3: Mutation rules

The block scheme of the genetic algorithm inspired by [32] is shown in the picture 4.4.

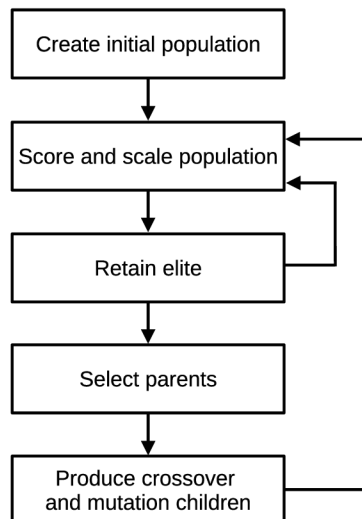


Fig. 4.4: Block scheme of generic algorithm

## 4.2 Decision tree

The decision tree is a supervised learning method. This method is one of the most effective methods for data mining and is used for classification and regression. The decision tree's goal is to create a model that predicts the results by learning simple decision rules. These decision rules are learned from the data features. [35]

The features can be created either from the measured data or from the data calculated by the LPTN. It is possible to use the decision tree for the fast pretending of machine behavior. Based on this fast pretending it is possible to find trends of the machine optimizing.

This method is easy to use, free of ambiguity, and does not need much computing power and time. The decision tree is very useful for quick identification of the result based on the input data and requires just a little data preparation, unlike the other methods. The decision tree is also very good in solving problems that are similar to the models used for learning. [35]

On the other hand, too complex trees might be created that do not generalize the data well. This phenomenon is called overfitting, and it is necessary to avoid it. It can be done in several ways, like setting the minimum number of samples required at a leaf node or setting the maximum depth of the tree. [35]

The decision trees are according to [36] common usage for:

- Variable selection
- Assessing the relative importance of variables
- Handling of missing values
- Prediction

- Data manipulation

The example of the created decision tree is shown as a block diagram in the picture 4.5. This diagram shows the single binary target variable  $Y$  and two continuous variables  $X_1$  and  $X_2$ . Every combination of input and variables return defined output  $R$ .

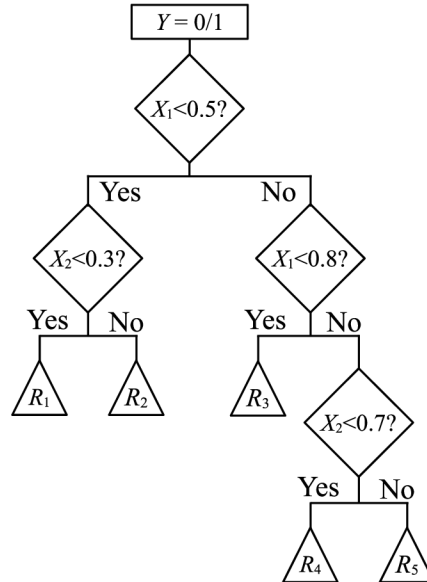


Fig. 4.5: Block diagram of decision tree

The decision trees are composed of the nodes and branches, as it is observed in the picture 4.5.

### 4.2.1 Nodes

There are three types of nodes in the decision tree construction. The first type of node represents a choice that divides all records into two or more mutually exclusive subsets. This node is called the decision node or also root node.

The second node type is called an internal node or a chance node. This node represents one of the possible choices available at the point in the tree structure. The top of the node is connected to the parent node and the bottom of it is connected to its child or leaf nodes.

The third type represents the final result of the decision tree or event combination. These nodes are called either leaf nodes or end nodes.

### 4.2.2 Branches

The decision tree structure is formed by using a hierarchy of branches. The branches represent random results or occurrences resulting from root or internal nodes. The

paths between the root node through internal nodes to a leaf node represent a decision rule. These paths can also be represented as the "if" rule.

For building the decision tree three most important steps are necessary.

### **4.2.3 Splitting**

Splitting is applied to parent nodes. These nodes are divided into purer child nodes. The splitting rule is used until only homogeneous nodes are reached. Both discrete input and continuous input variables can be used in the splitting of nodes. [36]

### **4.2.4 Stopping**

The stopping criteria are for the decision tree necessary. It is because these criteria keep the tree from being too complex. If the decision tree becomes too complex, it loses its ability to predict future cases accurately. That means the tree would have really poor generalization. [36], [37]

### **4.2.5 Pruning**

Because the stopping rules do not have to work very well in some situations, pruning is alternative to stopping the decision tree. This alternative of decision tree creation builds the large tree first, and then this tree is optimized to the optimal size by removing nodes that provide less additional information. [36]

## 5 Analysed machine

The nominal values of the analysed machine are shown in the table 5.1. The datasheet of the machine is shown in appendix A

Motor under test		Unit
Rated DC bus voltage	24	[V]
Rated DC bus current	5.1	[A]
Number of phases	3	[-]
Number of pole pairs	2	[-]
Phase connection	$\Delta$	[-]
Rated speed	7100	[rpm]
Rated torque	150	[mNm]
Resistance at 20°C	0.427	[ $\Omega$ ]

Tab. 5.1: Table of machine nominal values

There is shown the area where the temperatures of the machine are measured in the picture 5.1. The machine is monitoring in this area. This area is called SOAR (Safety operating area). The right upper corner of this area is the nominal machine point. With the increasing machine load moment, the stator current increases. So the linear decrease of the upper line is due to voltage drop. The stator resistance defines the gradient of this line.

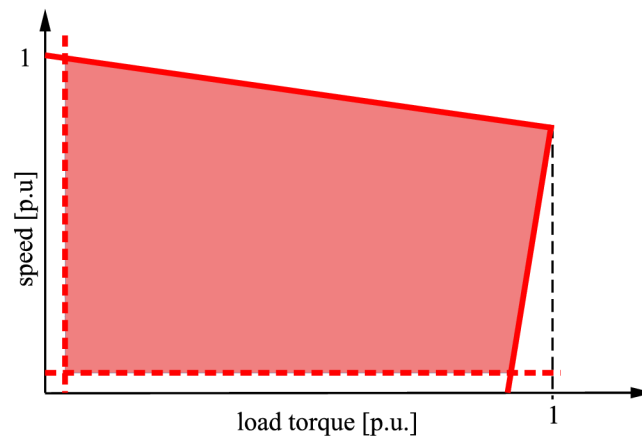


Fig. 5.1: Testing area

The vertical dashed line defines a lower speed limit measurable by hall sensors. The minimal torque is defines by the horizontal dashed line due to the losses of all component systems like air friction, bearing friction, etc.

There were two methods used for the temperatures measuring. First, the thermal

sensors were used for the measurement, that is, the direct measurement method. There are used seven sensors in the machine. These were placed at the surfaces of single-phase coils ( $T_{uv}$ ,  $T_{vw}$  and  $T_{wu}$ ), at the top of one pole of stator yoke ( $T_{air}$ ), on the outer static ring of the inner bearing ( $T_{bi}$ ), on the outer ring of the outer bearing ( $T_{bo}$ ) and on the mounting flange of machine ( $T_f$ ).

Second, the thermal camera have been used. Using the thermal camera is an indirect method of thermal measurement. It is necessary to use the indirect thermal measurement method if the measured part is moving. A typical example of this part is the rotor. There is used the thermal camera measures the temperature on its outer side ( $T_r$ ).

There are shown the measured temperatures in the part a) of the picture 5.2. In the part b) of this picture, the measured duty cycle is shown. This duty cycle is defined to cover the operating conditions that the machine can reach.

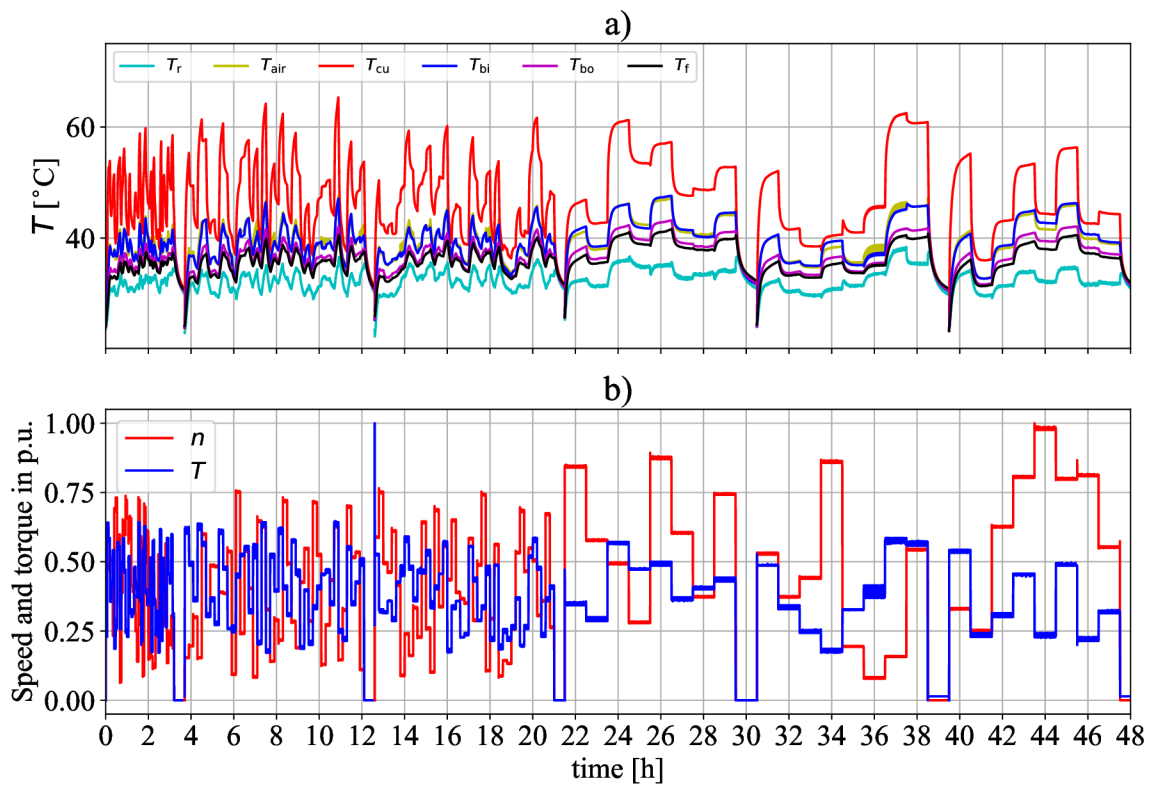


Fig. 5.2: Measured temperatures and duty cycle

The main goal of the thesis is to optimize convection thermal resistances. That means the values of the conduction resistances were also taken from the [23] and are shown in the table 5.2.



Tab. 5.2: Table of started conductivity resistances

Conductive resistance at 20°C	Value	Unit
$R_{sf,0}$	7.503	[KW <sup>-1</sup> ]
$R_{sair,0}$	2.409	
$R_{cus,0}$	2.750	
$R_{sbi,0}$	3.462	
$R_{bio,0}$	1.558	

## 5.1 Thermal network

There is shown the thermal network used for the temperature calculating in the picture 5.3. This LPTN is taken from the [23]. There are optimized parameter of this thermal network in this thesis.

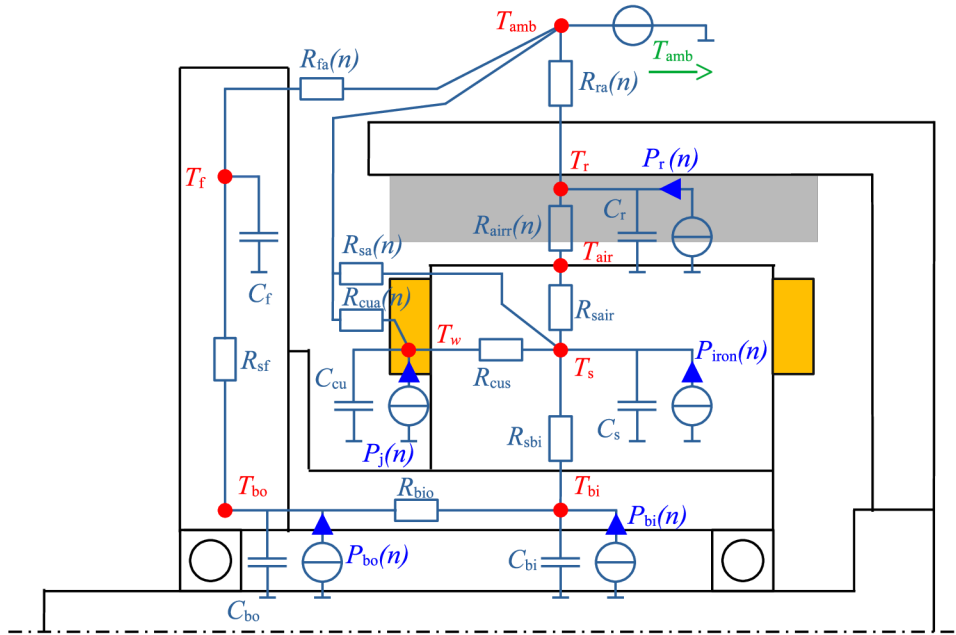


Fig. 5.3: Thermal network

## 6 Thermal analysis

This chapter is focused on the application of the described optimizing methods. First the genetic algorithm is applied on the thermal network and then the decision tree is used.

### 6.1 Application of the genetic algorithm

There are the results of the heat transfer coefficient calculated in nodes of the thermal network where the convective heat transfer is considered in the table 6.1. These results are calculated through the genetic optimization based on the formulas (3.16) and (3.18).

Tab. 6.1: Table of optimized linear and quadratic heat transfer coefficients

Node	Parameter	Linear value	Quadratic value	Unit
$T_f$	$h_{0,f}$	14.056	13.336	$[\text{Wm}^{-2}\text{K}^{-1}]$
	$h_{\delta,f}$	8.143	5.847	[-]
	$k_{f,s}$	0.547	0.628	
$T_r$	$h_{0,r}$	18.000	18.000	$[\text{Wm}^{-2}\text{K}^{-1}]$
	$h_{\delta,r}$	4.965	5.524	[-]
	$k_{r,s}$	0.127	0.379	
$T_s$	$h_{0,s}$	8.000	8.000	$[\text{Wm}^{-2}\text{K}^{-1}]$
	$h_{\delta,s}$	8.042	5.341	[-]
	$k_{s,s}$	0.484	0.724	
$T_{\text{cua}}$	$h_{0,\text{cua}}$	9.018	7.002	$[\text{Wm}^{-2}\text{K}^{-1}]$
	$h_{\delta,\text{cua}}$	5.112	5.055	[-]
	$k_{\text{cua},s}$	0.101	0.207	
$T_{\text{air}}$	$h_{0,\text{air}}$	3.945	3.889	$[\text{Wm}^{-2}\text{K}^{-1}]$
	$h_{\delta,\text{air}}$	7.199	5.276	[-]
	$k_{\text{air},s}$	0.515	0.642	

There are shown measured and calculated temperatures for the linear heat transfer coefficient approximation in the part a) of the figure 6.1. This figure observes how different the measured and calculated temperatures are. The calculated temperatures have almost the identical waveforms as the measured temperatures. The designed thermal model is very similar to the real measured machine.

In the part b) of the same picture, the absolute difference between the calculated

and measured temperatures is shown. The value of a total residuum for all data is equal to 1.037°C. The residuum defines according to [33] the deviation of the measured and calculated values, so-called the mean squared error. The residuum can be according to [34] calculated as

$$\varepsilon = \frac{1}{n} \sum_{i=1}^n (\hat{T} - \hat{T}_m)^2, \quad (6.1)$$

where the  $n$  is a number of measured points, the  $\hat{T}$  is the calculated temperature, and the  $\hat{T}_m$  is the measured temperature.

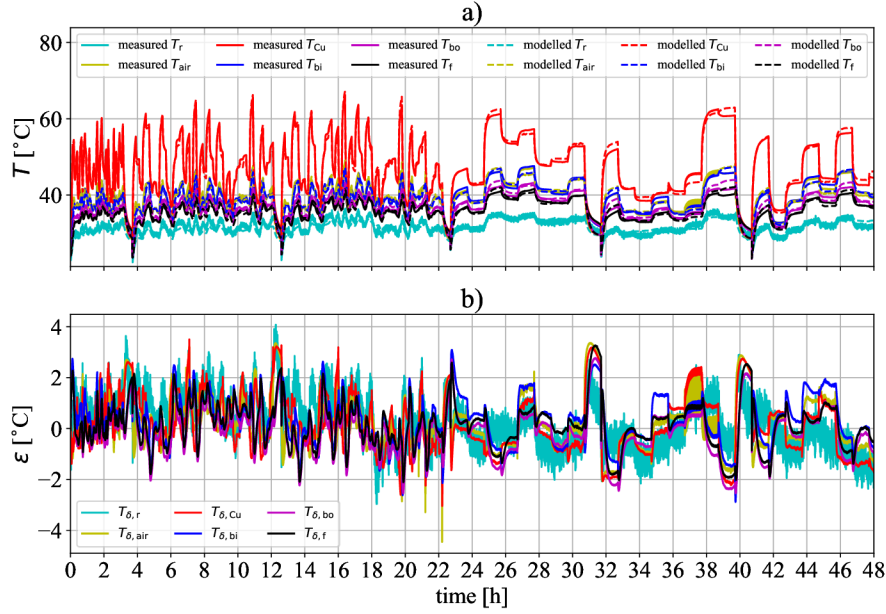


Fig. 6.1: Graphs based on linear heat transfer coeff. calculated by the GA

If the optimization of the quadratic heat transfer coefficient approximation is considered, the final temperature waveforms are shown in the part a) of the picture 6.2. The absolute differences between measured and calculated temperatures are shown in part b) of the same picture. The value of the total residuum is equal to 0.957°C.

Optimizing both the linear and quadratic heat transfer approximation gives us accurate results. The optimization of the linear approximation takes 47.86 hours, and the quadratic approximation takes 49.46 hours with the same set of initial population (200) and maximal numbers of the iterations (2000).

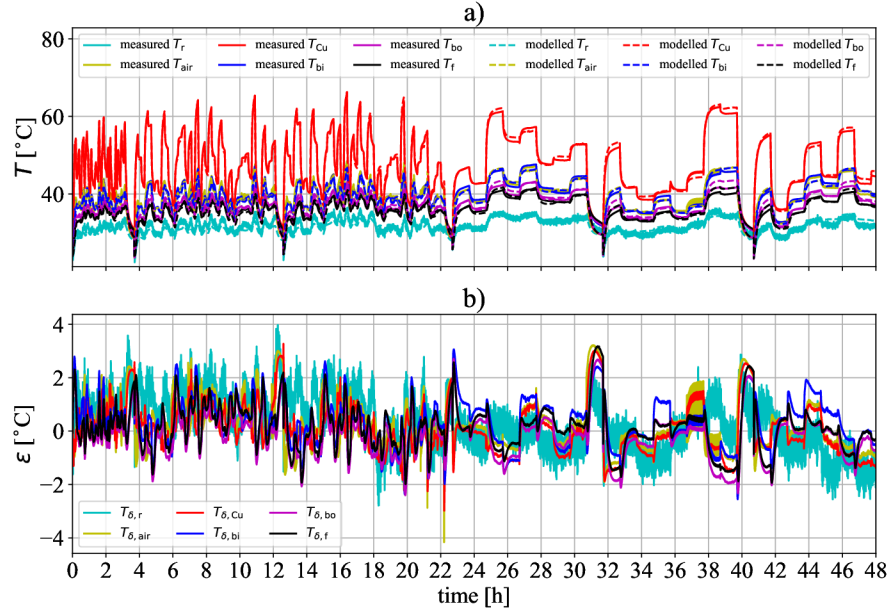


Fig. 6.2: Graphs based on quadratic heat transfer coeff. calculated by the GA

The results of genetic optimization calculated using the formula (3.19) are shown in the table 6.2. These results are calculated in the same nodes as in table 6.1.

Tab. 6.2: Table of optimized heat transfer coefficients calculated by the (3.19)

Node	Parameter	Value	Unit
$T_f$	$c_{1,f}$	15.000	$[\text{Wm}^{-2}\text{K}^{-1}]$
	$c_{2,f}$	0.022	[-]
	$c_{3,f}$	0.702	
$T_r$	$c_{1,r}$	12.583	$[\text{Wm}^{-2}\text{K}^{-1}]$
	$c_{2,r}$	0.050	[-]
	$c_{3,r}$	0.736	
$T_s$	$c_{1,s}$	7.183	$[\text{Wm}^{-2}\text{K}^{-1}]$
	$c_{2,s}$	0.020	[-]
	$c_{3,s}$	0.700	
$T_{cua}$	$c_{1,cua}$	4.622	$[\text{Wm}^{-2}\text{K}^{-1}]$
	$c_{2,cua}$	0.153	[-]
	$c_{3,cua}$	0.775	
$T_{air}$	$c_{1,air}$	22.000	$[\text{Wm}^{-2}\text{K}^{-1}]$
	$c_{2,air}$	0.646	[-]
	$c_{3,air}$	0.987	

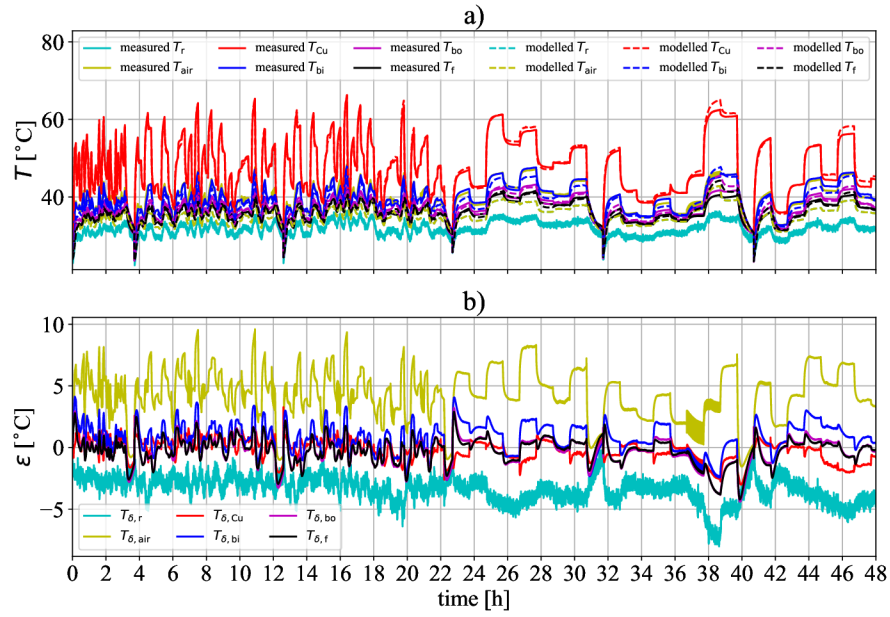


Fig. 6.3: Graphs calculated by genetic algorithm approximation using (3.19)

There are observed the waveforms of the calculated and measured temperatures in the part a) of the picture 6.3. The absolute differences between the calculated and measured temperatures are shown in part b) of the same picture.

The total calculated residuum of the temperatures is equal to  $2.592^{\circ}\text{C}$ . The total computation time was 46.28 hours, with the initial population equal to 200 and a maximal number of the iterations equal to 2000. The results calculated by all three approximations of conduction heat transfer are discussed more precisely in the 7.1.

## 6.2 Application of decision tree

The features are created from input data used for decision tree training. There are several ways the features can be created in this method, but the best way is to use the data that makes the physical sense in the field of the electrical machines. [38], [39] The physical parameters used for the feature creating are shown in the table 6.3

Tab. 6.3: Table of features used for the decision tree creating

Feautre	Used data
$f_1$	$n$
$f_2$	$n^2$
$f_3$	$n^3$
$f_4$	$I$
$f_5$	$I^2$
$f_6$	$In$

These features have been chosen because of the connection with the losses generated in the machine and the machine's cooling effects.

The speed of machine  $n$  influences bearing losses and capability of rotor cooling, and the current  $I_{ph}$  is related to the stator current losses. Moreover, these values are easy to measure, which predisposes them for the real-time estimation of the machine temperatures without the need for high calculating power.

### 6.2.1 Data preparing

In the case of measured data using it is convenient to use some filter for the features created. These filters are used to protect the decision tree before the poor learning due to interferences. In this thesis, two types of filters have been chosen:

- Moving average - MA
- Exponential moving average - EMA.

The moving average is, according to [40] the most common filter that can be used in DSP. It is because the moving average is easy to understand and use. This type of filter is good for reducing interferences of measured data. The formula for the moving average calculation is according to [40] defined as

$$x_n = \frac{y_n + y_{n+1} + y_{n+2} + \dots + y_{n+w}}{w}, \quad (6.2)$$

where the  $x_n$  is the averaged value of  $n^{\text{th}}$  sample, the  $y_n$  is the raw value of  $n^{\text{th}}$  data sample, and  $w$  is the number of values used to average so-called the window.

It is better to move the window into the past for the practical use of this data filtering method and use in DSP. That means the moving average works with the earlier measured data. This approach is used because the sensors measure the zeros when the machine is switched off. This shows the equation (6.3).

$$x_n = \frac{y_{n-w} + y_{n-w+1} + y_{n-w+2} + \dots + y_n}{w}. \quad (6.3)$$

The way how the moving average described by (6.3) works is shown in the picture 6.4. This method is suitable for the practical use as it is described upper.

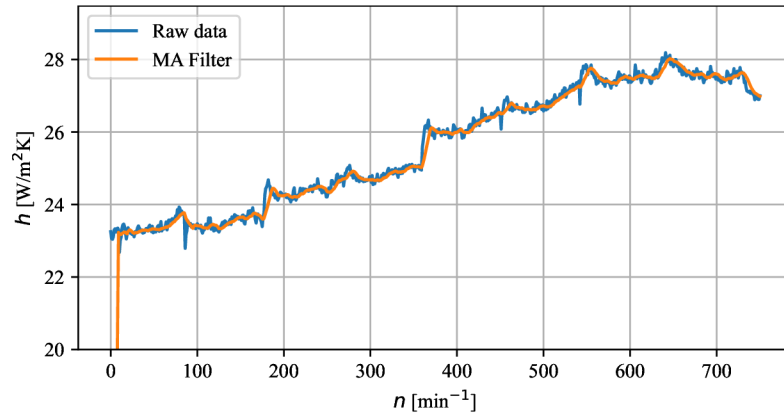


Fig. 6.4: Example of moving average filter using

Little troubles come when it is used for learning the decision tree. Multiple cycles connected in sequence bring biased values and might negatively influence learning. So there is a modification of the moving average calculation for the learning. That modification does not consider zeros in the first steps of the window, but the same value as the first value of the waveform is. Then the moving average looks like 6.5.

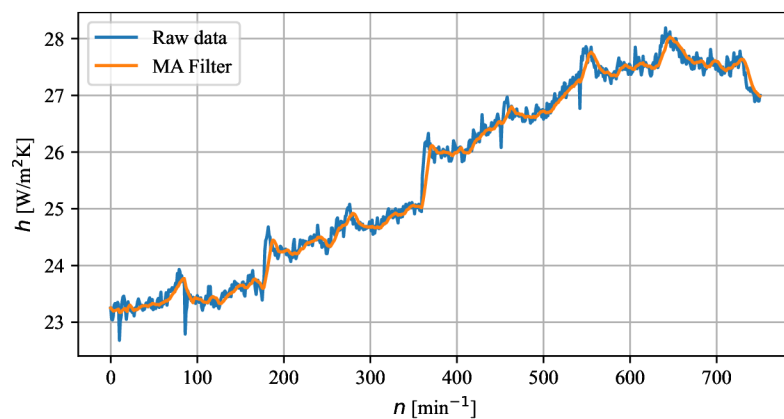


Fig. 6.5: Example of moving average filter using

The Exponential moving average is the averaging that gives more significance to points in the near past and less significant to points in the more distant past. The

difference between the exponential moving average and the moving average is the moving average gives the same weight for all considered points. [41], [42] According to [43] the exponential moving average can be calculated as

$$x_n = y_n \alpha (1 - \alpha) x_{n-1}, \quad (6.4)$$

where the  $\alpha = \frac{1}{w}$  and the  $x_{n-1}$  is previous calculated value.

Data filtered by the exponential moving average are shown in the picture 6.6.

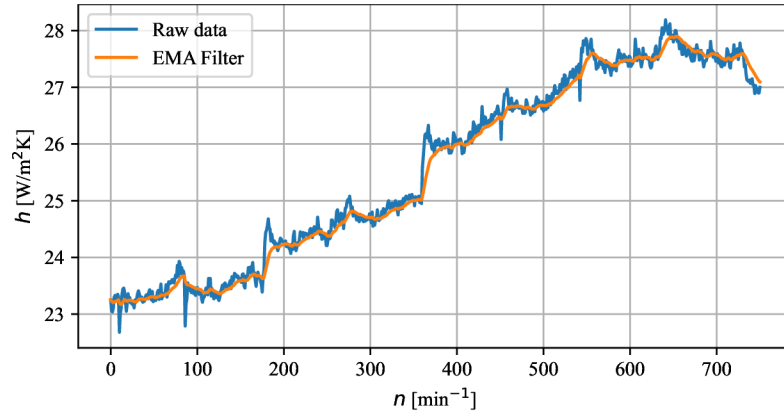


Fig. 6.6: Example of exponential moving average filter using

First, the raw data for the features creating have been used. The picture 6.7 shows measured temperatures and temperatures predicted at the same point of the duty cycle by the decision tree. These graphs show how the decision tree is good in its predictions. If all points are placed on the blue diagonal line, the decision is very accurate. This picture shows that the learned decision tree has poor accuracy in the prediction.



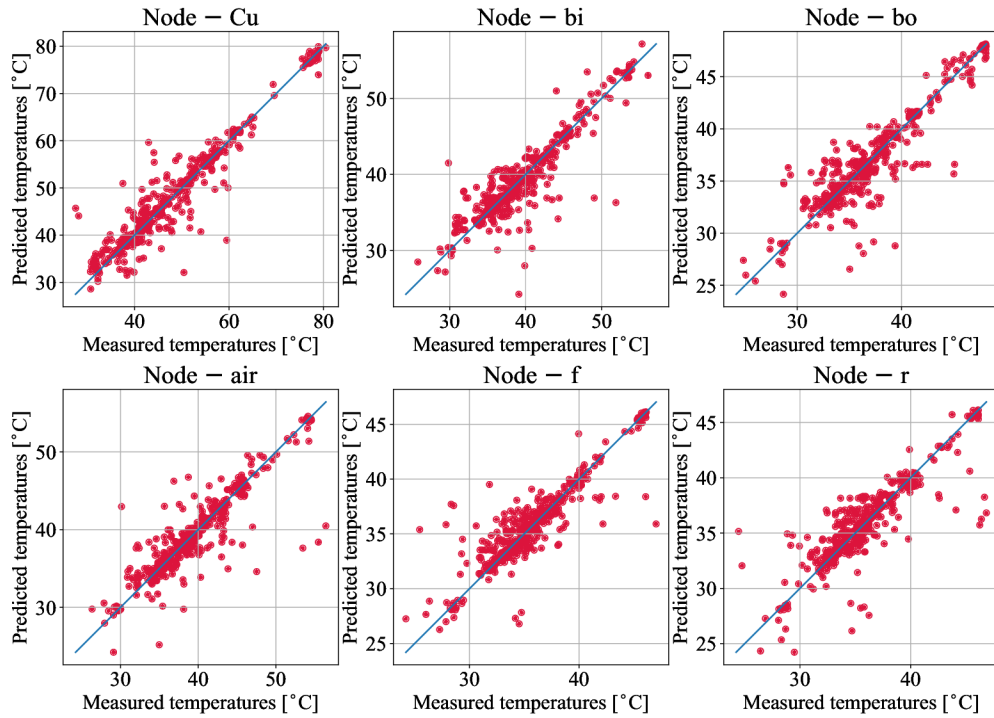


Fig. 6.7: Quality of the decision tree learning for raw data

In the light of the preceding information, not-good results of the temperature waveforms are observed. The results of it are shown in the figure 6.8. The temperature waveforms are observed in the part a) of this picture. The part b) of this picture shows the differences between measured and predicted temperatures, what is the absolute difference of the calculation.

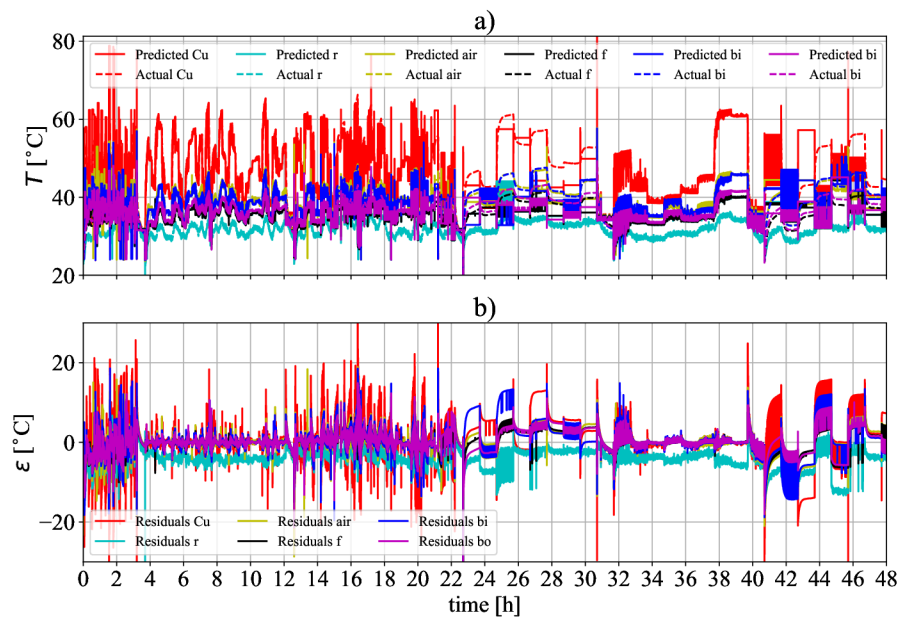


Fig. 6.8: Graphs calculated by decision tree using raw data

The values of the mean absolute errors of features used for the decision tree learning that is created by raw data in single nodes are shown in the table 7.2

In the picture 6.9 the results of the decision tree where is the moving average used for the creation features are observed. The prediction points are fit in the diagonal line better than in the case where the raw data are used. That means the decision tree learning is much better, and its predictions are more accurate in this case.

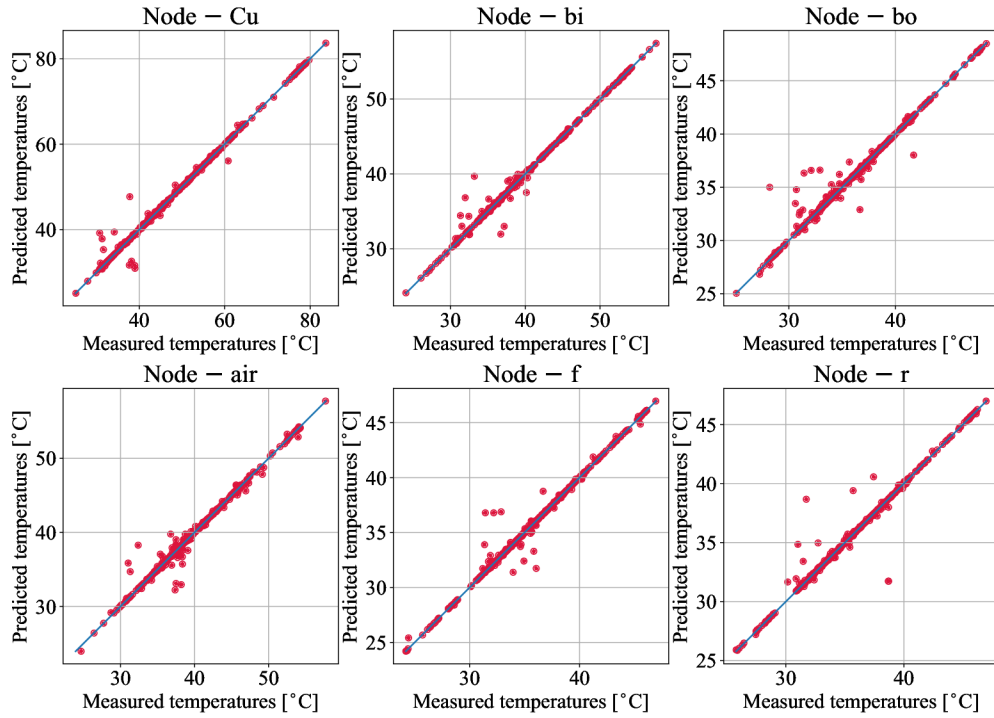


Fig. 6.9: Quality of the decision tree learning for MA filter

Thanks the better learning, the better results of temperature waveform predictions are expected. As it is shown in the part a) of the picture 6.10 the results from the decision tree are better. In the same picture, the part b) shown the absolute errors of temperatures. The values of the mean absolute difference when the moving average filter is used for the feature creation are in the table 7.2.

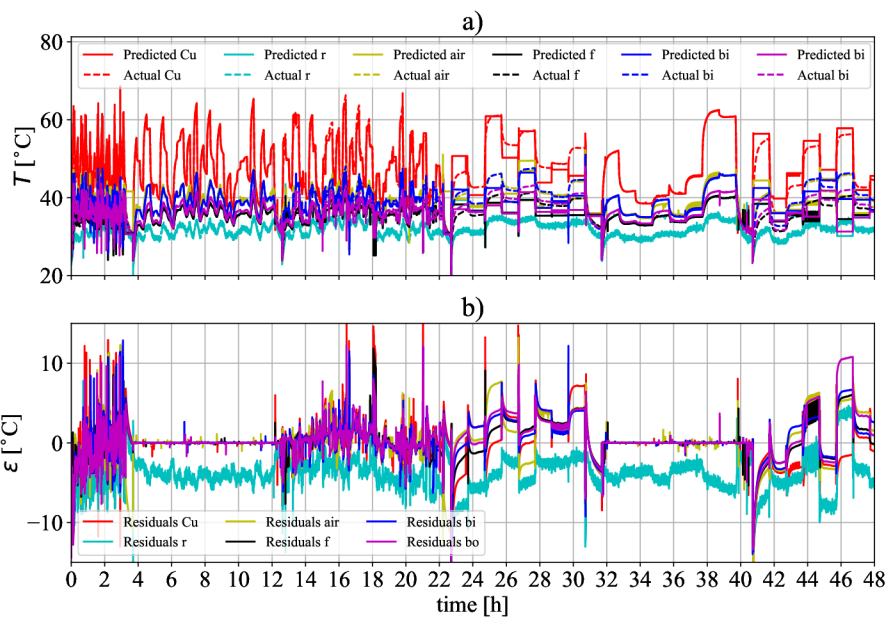


Fig. 6.10: Graphs calculated by decision tree using MA filtered data

The results of decision tree learning observed in the picture 6.11 show how good the tree is. This decision tree used the features created by the exponential moving average. The prediction points are placed in the diagonal line much better than in both upper cases. That means a very accurate result of the temperature prediction can be expected.

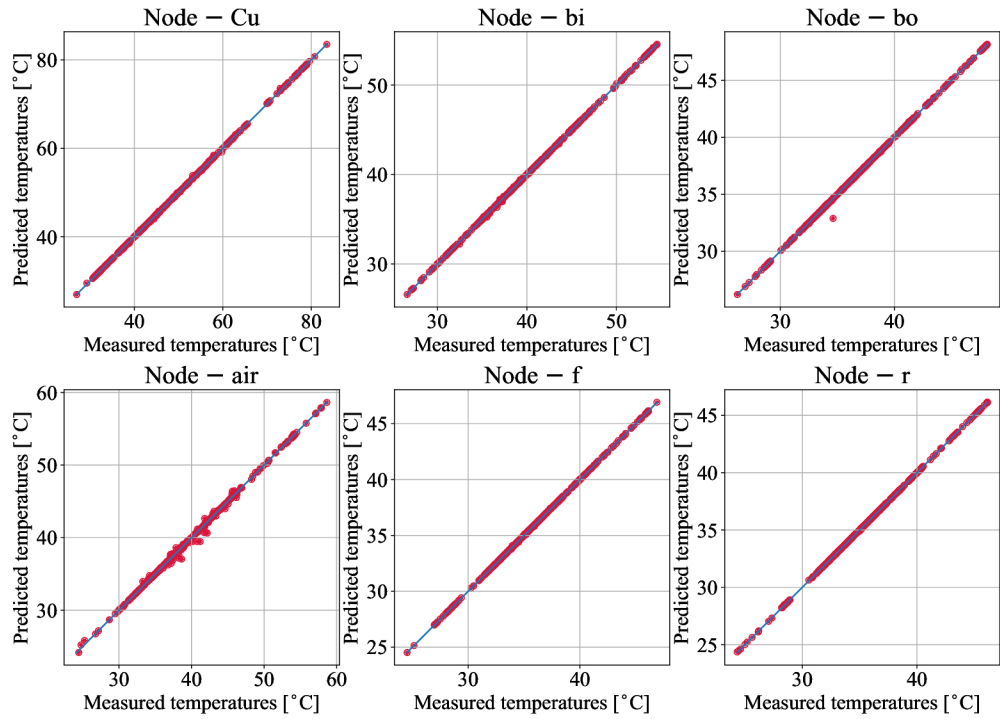


Fig. 6.11: Quality of the decision tree learning for EMA filter

There are shown the predicted and measured temperatures in the part a) of the picture 6.12. At first glance, it is evident that these predicted temperatures are very similar to the measured. The part b) of this picture observes the values of the absolute difference. The maximal absolute error is moving around  $5^{\circ}\text{C}$ , and the values of the mean absolute errors in single nodes are in the table 7.2. Both, the part a) and part b) confirms the assumptions based on the picture 6.11 and described upper.

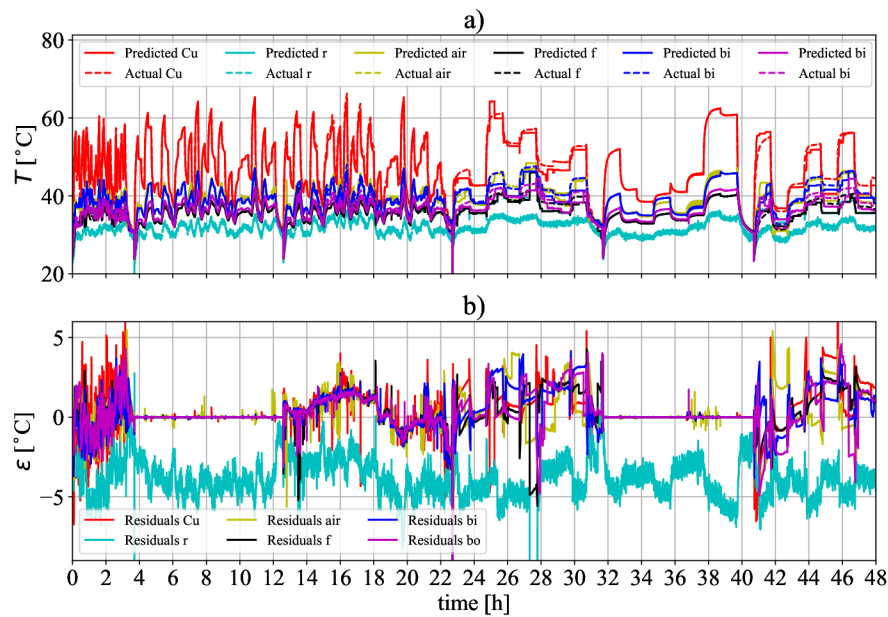


Fig. 6.12: Graphs calculated by decision tree using EMA filter

The results mined by all three iterations of the decision tree are discussed more precisely in the chapter 7.1.

## 7 Comparison of calculated results and measured data

This chapter is focused on the comparing measured data with the results mined from the calculations. Moreover, the usability for real-time calculation in terms of the computing time, necessary computing power, and accuracy is discussed in this chapter.

### 7.1 Data evaluation

The data calculated by the genetic algorithm are summarized in the table 7.1. This table shows the computation time and the accuracy of the calculated data. These parameters are crucial to evaluating the methods.

Tab. 7.1: Table of mean squared errors in single nodes

Node error	Linear	Quadratic	According to (3.19)	Unit
$\varepsilon_{Cu}$	1.201	0.955	0.863	C°
$\varepsilon_r$	0.931	0.870	1.038	
$\varepsilon_{air}$	1.077	0.973	4.653	
$\varepsilon_f$	0.931	0.870	1.503	
$\varepsilon_{bi}$	1.021	0.948	1.503	
$\varepsilon_{bo}$	0.936	0.869	1.110	
computing time	47.86	49.46	46.29	h

The table 7.1 shows that the approximation by (3.19) needs the lowest computing time, but computing accuracy is the worst. On the other hand, the best computing accuracy is reached by the quadratic approximation of conduction heat transfer. However, this approximation needs the highest computation time to calculate these results. In light of these parameters, the best way for the LPTN optimization is to use the linear approximation of conduction heat transfer. It is thanks the excellent accuracy of the calculations combined with the relatively short computing time.

If the error of calculations is lower than 5°C, it is considered a reasonable accuracy. An error lower than 2.5°C is a good accuracy, and the error around 1°C is the perfect accuracy of the calculations. These boundaries of accuracy are based on the accuracy classes of thermal used sensors. Thermal sensors with higher accuracy classes are more expensive, so the balance between cost and accuracy class is necessary to find.

So it is necessary to say that all three ways of conducting heat transfer approximation give very good results in terms of the computing time and also calculating accuracy. That means the way of approximation depends on the requirements for the temperature estimation accuracy of the specific machine application. If either the perfect LPTN or the cheaper calculation of it is needed.

There are the mean absolute error results mined by the decision tree in the table 7.2. The errors are calculated for the same nodes as the temperatures in the case of the genetic algorithm.

The table 7.2 shows that the worst accuracy of the calculated temperatures was reached when the raw data were given for the decision tree learning. As discussed, it is because the raw measured data are rippled, which might negatively influence the ability of the tree to learn. Better accuracy of the calculation is reached if the moving average filter for the creating features is used. It is because the data used for the learning are smoothed, and the learned decision tree can better predict the temperatures. This table also shows that the best predictions are reached if the exponential moving average is used for the feature creation. First of all, it is because the data are smoothed, but it is also because the exponential moving average is better to fit the reality. The better reality fit of this averaging consists in the different weights of the data.

Tab. 7.2: Table of mean squared errors in single nodes

Node error	No filter	MA	EMA	Unit
$\varepsilon_{Cu}$	11.255	0.586	0.020	C°
$\varepsilon_r$	3.087	0.102	0.007	
$\varepsilon_{air}$	4.793	0.171	0.042	
$\varepsilon_f$	5.946	0.501	0.002	
$\varepsilon_{bi}$	3.101	0.656	0.008	
$\varepsilon_{bo}$	2.853	0.376	0.0004	

The computation time for all ways of learning is in the order of minutes. However, the main disadvantage of the decision trees over the genetic algorithms is the inability of data extrapolating. So the decision trees are much faster than the genetic algorithms. For this reasons, the trees are perfect for predictions of very similar situations to which have been learned.

So the decision tree can predict very accurate temperatures but needs many data to learn. Thanks the low computing power requirements, the realization of the real-time calculation is much easier.

On the other hand, the genetic algorithm needs more computing time and computing power. However, the LPTN optimized by the genetic algorithm has a really

good ability to precisely predict the temperatures of the machine even if an unknown state occurs. So the main power of the LPTN optimized by the genetic algorithm is precisely calculations of temperatures for almost any possible state of the machine. Final LPTN optimized for a given machine does not need much computing time and power, but the decision trees still need less. So the realization of real-time temperature computing is more complex.

The main advantage of real-time temperature calculation is the absence of thermal sensors placed in machines. This advantage is practical, particularly in the low-cost machine segment. It is because thermal sensors with high tolerance class cost about 10 € and for measurement of this machine temperatures are seven sensors needed. The tolerances of this tolerance class are around  $\pm 0.35\%$  at  $100^{\circ}\text{C}$ , depending on the maker of the sensor. Sensors with a low tolerance class cost about 1-2 €. The tolerance of it at  $100^{\circ}\text{C}$  is about  $\pm 1.6\%$  again depending on the maker of the sensor. Moreover, there is necessary to modify the machine for the sensors placing and an evaluation of electronics is needed.

The real-time modeling needs only input data, particularly the machine's input current and speed. The input current is usually known, especially if the frequency converter for controlling is used. The speed of the machine is also measured or calculated as output because of system requirements. Then the DPS to calculate the actual temperature of the machine is needed.

# Conclusion

At first, thesis deals with the classification of synchronous machines of design was described. In this part of the thesis, the overview of inner rotor machines and outer rotor machines is made. Moreover, in chapter 1.2 is explained principle of the synchronous machine function.

Then the analysis of losses generated in permanent magnet synchronous machines and dividing of these losses are explained. The right analysing of the losses is a very important part of thermal dimensioning. Also, the losses generated by fluid flowing over the moving rotor and its calculation are described in this thesis.

In the middle of the thesis the mechanisms of heat transfer were explained. The heat transfer considers only three defined mechanisms which are conduction, convection, and radiation. The cooling of the machines is due to these mechanisms only. There were also described principles of direct and indirect machines cooling systems. In the same chapter were also described ways of convection heat transfer and convection thermal resistances approximations. These approximations were used in the LPTN. This LPTN was also used for the temperature estimation.

Moreover, there were described and used methods for the thermal network parameters optimizing. The parameters of LPTN were optimized by the genetic algorithm to better approximation of the real machine. Another described method of temperature estimation is the decision tree. This method was evaluated as method with the lower computing time and lower necessary computing power so it is suitable for the real-time machine temperature estimation.

There was shown the measured duty cycle with the measured temperatures in the picture 5.2 at the end of the thesis. There were also tables 7.1 and 7.2 with the summarizing of the mean squared errors. Then the evaluation in terms of computing time and computing power of those methods were done.

Temperatures calculated by both methods were graphically plotted. These plottings of temperatures estimated by the genetic algorithm were shown in the pictures 6.1,6.2 and 6.3. The temperatures estimated by the decision tree were plotted in the pictures 6.8,6.10 and 6.12. In those picture were also plotted the absolute error between the measured and calculated temperatures.



# Bibliography

- [1] PYRHÖNEN, Juha, Valeria HRABOVCOVÁ a Scott SEMKEN. *Electrical machine drives control: an introduction*. Chichester, West Sussex, United Kingdom: John Wiley & Sons, [2016]. ISBN 9781119260455.
- [2] SEN, P. C. *Principles of electric machines and power electronics*. Third edition. Hoboken: John Wiley and Sons, [2014]. ISBN 978-1-118-07887-7.
- [3] LEVKIN, Dmitry. Permanent magnet synchronous motor. *Engineering-solutions* [online]. 2021 [cit. 2022-01-05]. Available from: <https://en.engineering-solutions.ru/motorcontrol/pmsm/>
- [4] D. Wöckinger et al., "Measurement-Based Optimization of Thermal Networks for Temperature Monitoring of Outer Rotor PM Machines," 2020 IEEE Energy Conversion Congress and Exposition (ECCE), 2020, pp. 4261-4268, doi: 10.1109/ECCE44975.2020.9236388.
- [5] Taha, Harwan & Alnaab, Ismaeil. (2019). Designs of PMSMs with Inner and Outer Rotors for Electric Bicycle Applications. *Kurdistan Journal of Applied Research*. 4. 20-25. 10.24017/science.2019.1.4.
- [6] D. Yu, X. Huang, J. Ma and Y. Fang, "A comparative study on two outer rotor PMSMs for in-wheel direct drive under short-circuit faults," 2017 20th International Conference on Electrical Machines and Systems (ICEMS), 2017, pp. 1-5, doi: 10.1109/ICEMS.2017.8055919.
- [7] PYRHÖNEN, Juha, Tapani JOKINEN a Valéria HRABOVCOVÁ. *Design of Rotating Electrical Machines*. 2nd Edition. New Delhi, India: Library of Congress Cataloging-in-Publication Data, 2013. ISBN ISBN: 978-1-118-58157-5.
- [8] BLAHOVEC, Antonín. *Základy elektrotechniky v příkladech a úlohách*. Praha: Státní nakladatelství technické literatury, 1989. ISBN 80-03-00108-0.
- [9] TAGHIZADEH KAKHKI, Mehdi. *Modeling of losses in a permanent magnet machine fed by a PWM supply* [online]. Québec, Canada, 2016 [cit. 2022-01-05]. Available from: <https://corpus.ulaval.ca/jspui/bitstream/20.500.11794/27358/1/33161.pdf>. Doctoral Thesis. UNIVERSITÉ LAVAL.
- [10] H. Domeki et al., "Investigation of benchmark model for estimating iron loss in rotating machine," in *IEEE Transactions on Magnetics*, vol. 40, no. 2, pp. 794-797, March 2004, doi: 10.1109/TMAG.2004.825442

- [11] Eddy Current Loss Formula. *Electrical Volt* [online]. 2021 [cit. 2022-01-05]. Available from: <https://www.electricalvolt.com/2019/08/eddy-current-loss-formula/>
- [12] P. A. Hargreaves, B. C. Mecrow and R. Hall, "Calculation of iron loss in electrical generators using finite element analysis," 2011 IEEE International Electric Machines & Drives Conference (IEMDC), 2011, pp. 1368-1373, doi: 10.1109/IEMDC.2011.5994805.
- [13] K. Yamazaki, "Efficiency analysis of induction motors for ammonia compressors considering stray load losses caused by stator and rotor slot ripple," Conference Record of the 2001 IEEE Industry Applications Conference. 36th IAS Annual Meeting (Cat. No.01CH37248), 2001, pp. 762-769 vol.2, doi: 10.1109/IAS.2001.955531.
- [14] W. Guan et al., "Numerical Modeling of Excess Loss in SiFe Sheet Considering Pinning Effect," in IEEE Transactions on Applied Superconductivity, vol. 26, no. 7, pp. 1-4, Oct. 2016, Art no. 0608804, doi: 10.1109/TASC.2016.2597167.
- [15] *SKF* [online]. 2015 [cit. 2022-01-05]. Available from: <https://www.skf.com/group/support/splash>
- [16] Gieras, Jacek & Wang, Rong-Jie & Kamper, Maarten. (2008). Axial Flux Permanent Magnet Brushless Machines. 10.1007/978-1-4020-8227-6.
- [17] SAARI, Juha. *Thermal analysis of high-speed induction machines* [online]. Acta Polytechnica Scandinavica, 1998 [cit. 2022-01-05]. Available from: <http://urn.fi/urn:nbn:fi:tkk-001237>. Dizertační práce. Helsinki University of technology, Laboratory of Electromechanics.
- [18] CENGEL, Yunus A. a Afshin J. GHAJAR. *HEAT AND MASS TRANSFER: FUNDAMENTALS APPLICATIONS*. 5th edition. New York: McGraw-Hill Education, 2015. ISBN 978-0-07-339818-1.
- [19] LÁZNIČKOVÁ, Ilona. *Technická mechanika: Mechanika poddajných těles*. Fakulta elektrotechniky a komunitkačních technologií: VUT v Brně, 2014.
- [20] TOMAN, Marek. *VÁZANÉ MODELOVÁNÍ ASYNCHRONNÍHO MOTORU METODOU FYZIKÁLNÍHO MODELOVÁNÍ*. Antonínská 548/1, 601 90 Brno, 2015. Diplomová práce. Vysoké učení technické v Brně, Fakulta elektrotechniky a informačních technologií. Vedoucí práce Doc. Ing. RADEK VLACH, Ph.D.

- [21] Conduction Heat Transfer. *Engineering Library* [online]. U.S. Department of Energy: U.S. Department of Energy, 1992, 2021 [cit. 2021-04-18]. Available from: <https://engineeringlibrary.org/reference/conduction-heat-transfer-doe-handbook>
- [22] SCHAUER, Pavel. *Aplikovaná fyzika* [online]. Antonínská 548/1, 2014 [cit. 2019-10-31]. Available from: [http://lences.cz/domains/lences.cz/skola/subory/Skripta/BB02-Aplikovana%20fyzika/BB02-Aplikovana\\_fyzika\\_\(A,K\)--M04-Prenos\\_tepla.pdf.Skripta.VUTvBrně](http://lences.cz/domains/lences.cz/skola/subory/Skripta/BB02-Aplikovana%20fyzika/BB02-Aplikovana_fyzika_(A,K)--M04-Prenos_tepla.pdf.Skripta.VUTvBrně).
- [23] D. Wöckinger et al., "Approaches for Improving Lumped Parameter Thermal Networks for Outer Rotor SPM Machines," 2021 IEEE Energy Conversion Congress and Exposition (ECCE), 2021, pp. 3821-3828, doi: 10.1109/ECCE47101.2021.9594930.
- [24] Dirac delta function. In: *Wikipedia: the free encyclopedia* [online]. San Francisco (CA): Wikimedia Foundation, 2001- [cit. 2022-05-17]. Dostupné z: [https://en.wikipedia.org/wiki/Dirac\\_delta\\_function](https://en.wikipedia.org/wiki/Dirac_delta_function)
- [25] R. Ibtouen, S. Mezani, O. Touhami, N. Nouali and M. Benhaddadi, "Application of lumped parameters and finite element methods to the thermal modeling of an induction motor," IEMDC 2001. IEEE International Electric Machines and Drives Conference (Cat. No.01EX485), 2001, pp. 505-507, doi: 10.1109/IEMDC.2001.939354.
- [26] B. Assaad, K. El kadri Benkara, G. Friedrich, S. Vivier and A. Michon, "Reducing the complexity of thermal models for electric machines via sensitivity analyses," 2017 IEEE Energy Conversion Congress and Exposition (ECCE), 2017, pp. 4658-4665, doi: 10.1109/ECCE.2017.8096795.
- [27] BOGLIETTI, Aldo a Andrea CAVAGNINO. Analysis of the Endwinding Cooling Effects in TEFC Induction Motors. *IEEE Transactions on Industry Applications* [online]. 2007, **43**(5), 1214-1222 [cit. 2022-05-02]. ISSN 0093-9994. Available from: doi:10.1109/TIA.2007.904399
- [28] G. E. Luke, "The Cooling of Electric Machines," in Transactions of the American Institute of Electrical Engineers, vol. XLII, pp. 636-652, January-December 1923, doi: 10.1109/T-AIEE.1923.5060903.
- [29] B. Fahimi et al., "Guest Editorial Optimal Design of Electric Machines," in IEEE Transactions on Energy Conversion, vol. 30, no. 3, pp. 1143-1143, Sept. 2015, doi: 10.1109/TEC.2015.2458232.

- [30] G. Bramerdorfer, J. A. Tapia, J. J. Pyrhönen and A. Cavagnino, "Modern Electrical Machine Design Optimization: Techniques, Trends, and Best Practices," in *IEEE Transactions on Industrial Electronics*, vol. 65, no. 10, pp. 7672-7684, Oct. 2018, doi: 10.1109/TIE.2018.2801805.
- [31] Genetic Algorithms. *GeeksforGeeks* [online]. Noida, 22.2.2022 [cit. 2022-03-26]. Available from: <https://www.geeksforgeeks.org/genetic-algorithms/>
- [32] *MathWorks* [online]. The MathWorks, 1994 [cit. 2022-03-26]. Available from: [https://www.mathworks.com/?s\\_tid=gn\\_logo](https://www.mathworks.com/?s_tid=gn_logo)
- [33] *Statistics how to.com* [online]. 2022 [cit. 2022-05-08]. Available from: <https://www.statisticshowto.com/>
- [34] Machine learning: an introduction to mean squared error and regression lines. *FreeCodeCamp.org* [online]. USA, 2018 [cit. 2022-05-11]. Available from: <https://www.freecodecamp.org/news/machine-learning-mean-squared-error-regression-line-c7dde9a26b93/>
- [35] Decision Trees. *Scikit-learn: Machine Learning in Python* [online]. 2007 [cit. 2022-05-02]. Available from: <https://scikit-learn.org/stable/modules/tree.html>
- [36] SONG, Yan-yan a Ying LU. Decision tree methods: applications for classification and prediction. *National library of medicine* [online]. 2015, 24.4.2015, 130—135 [cit. 2022-05-02]. Available from: doi:10.11919/j.issn.1002-0829.215044
- [37] Decision trees in more detail. *Clustering and Classification methods for Biologists* [online]. Menchester Metropolitan University: Menchester Metropolitan University [cit. 2022-05-02]. Available from: [http://www.alanfielding.co.uk/multivar/crt/dt\\_example\\_04.htm](http://www.alanfielding.co.uk/multivar/crt/dt_example_04.htm)
- [38] *Towards Data Science* [online]. Towards Data Science, 2018 [cit. 2022-05-02]. Available from: <https://towardsdatascience.com/decision-tree-in-machine-learning-e380942a4c96>
- [39] TAHIR, Nooritawati Md, Aini HUSSAIN, Salina Abdul SAMAD, Khairul Anuar ISHAK a Rosmawati Abdul HALIM. Feature Selection for Classification Using Decision Tree. *2006 4th Student Conference on Research and Development* [online]. IEEE, 2006, 2006, 99-102 [cit. 2022-05-02]. ISBN 978-1-4244-0526-8. Available from: doi:10.1109/SCORED.2006.4339317

- [40] SMITH, Steven W. Moving Average Filters. *Digital Signal Processing* [online]. Elsevier, 2003, 2003, 277-284 [cit. 2022-04-27]. ISBN 9780750674447. Available from: doi:10.1016/B978-0-7506-7444-7/50052-2
- [41] Understanding Moving Averages. *CME Group* [online]. 2022 [cit. 2022-04-27]. Available from: <https://www.cmegroup.com/education/courses/technical-analysis/understanding-moving-averages.html>
- [42] What is a Moving Average?. *CFI Education Inc.* [online]. 2015 [cit. 2022-04-27]. Available from: <https://corporatefinanceinstitute.com/resources/knowledge/other/moving-average/>
- [43] BURGSTAHLER, Lars a Martin NEUBAUER. *New Modifications of the Exponential Moving Average Algorithm for Bandwidth Estimation* [online]. Institute of Communication Networks and Computer Engineering: University of Stuttgart [cit. 2022-04-27]. Available from: [http://content.ikr.uni-stuttgart.de/Content/Publications/Archive/Bu\\_ITCSS15-49\\_34635.pdf](http://content.ikr.uni-stuttgart.de/Content/Publications/Archive/Bu_ITCSS15-49_34635.pdf)

# Symbols and abbreviations

$B$	Flux density
$B_m$	Flux density amplitude
$B_r$	Radial component of flux density
$B_x$	Flux density in the x-axis
$B_y$	Flux density in the y-axis
$B_\theta$	Peripheral component of flux density
$c_1$	Calculation coefficient
$L_s$	Calculation coefficient
$L_s$	Calculation coefficient
$C_{f,1}$	Friction coefficient
$C_{f,2}$	Friction coefficient
$C_{fb}$	Friction contact coefficient
$d$	Thickness of lamination
$d$	Thickness of the solid
$d_b$	Bearing bore diameter
$D_r$	Rotor diameter
$D_{s,in}$	Air gap outer diameter
$f$	Frequency
$EMA$	Exponential moving average
$F$	Equivalent dynamic bearing load
$FE$	Finite element method
$h_0$	Initial value of heat transfer coefficient
$h$	Heat transfer coefficient
$h_1$	Heat transfer coefficient

$h_{\text{lin}}$	Linear approximation of heat transfer coefficient
$h_{\text{q}}$	Heat transfer coefficient
$h_{\text{quad}}$	Linear approximation of heat transfer coefficient
$h_{\text{stat}}$	Static heat transfer coefficient
$h_{\delta}$	Static heat transfer coefficient
$i_{\text{d}}$	Current in the d-axis
$I_{\text{ph}}$	Phase current
$i_{\text{PM}}$	Current source
$R_{\text{Q}}$	Damper resistance
$i_{\text{s}}$	Stator current
$k_{\text{e}}$	Eddy current coefficient
$k_{\text{ed}}$	Eddy current loss coefficient
$k_{\text{ex}}$	Coefficient determined by curve fitting of the material
$k_{\text{fb}}$	Coefficient depend on the bearing specification
$k_{\text{h}}$	Experimental coefficient
$k_{\text{is}}$	Optimization coefficient
$k_{\text{ro}}$	Roughness coefficient of material
$L$	Cylinder length
$L$	Rotor length
$L_{\text{c}}$	Characteristic length
$L_{\text{D}}$	Total damper inductance in the d-axis
$L_{\text{D}\sigma}$	Damper linkage resistance
$LPTN$	Lumped parameter thermal network
$L_{\text{s}\sigma}$	Stator leakage inductance
$L_{\text{md}}$	Magnetizing inductance

$L_{mq}$	Magnetizing inductance
$L_Q$	Total damper inductance in the q-axis
$L_{Q\sigma}$	Damper leakage inductance
$L_s$	Stator length
$MA$	Moving average
$m_r$	Rotor mass
$N_p$	Number of steps per period
$Nu$	Nusselt number
$n_{\max}$	Maximal speed of machines
$n$	Rotor speed
$P$	Power of machine
$P_b$	Bearing mechanical losses
$p_{ir}$	Ratio between stator teeth iron volume and the total volume of stator iron
$Q_{\text{cond}}$	Transferred heat by conduction
$Q_{\text{conv}}$	Convection heat transfer
$Q_{\text{rad}}$	Radiation heat flow
$q$	Heat flux
$R_{\text{cond}}$	Conduction resistance
$R_{\text{cond,cyl}}$	Solid cylinder thermal resistance in radial direction
$R_{\text{cond,bar}}$	Cylinder thermal resistance in radial direction
$R_{\text{conv}}$	Convection thermal resistance
$R_D$	Damper resistance
$Re_\delta$	Reynolds number
$R_{\text{lin},i}(n)$	Linear approximation of speed-dependency thermal resistance



$R_{\text{ph},0}$	Phase resistance at 20°C
$R_{\text{ph}}$	DC resistance
$R_{\text{quad},i}(n)$	Quadratic approximation of speed-dependency thermal resistance
$R_{\text{s}}$	Stator resistance
$R_{\text{T}}$	Thermal resistance
$R_{i,0}$	Thermal resistance at zero speed
$r_1$	Cylinder inner radius
$r_2$	Cylinder outer diameter
$r$	Inner radius of rotor
$S$	Area
$S$	Heat transfer surface
$T_1$	Thermodynamic temperature of inner solid
$T_2$	Thermodynamic temperature of outer solid
$T$	Period, thermodynamic temperature
$T_{\text{air}}$	Temperature sensor of inner air
$T_{\text{e}}$	Generated torque of machine
$T_{\text{f}}$	Temperature sensor of flange
$T_{\text{bi}}$	Temperature sensor of inner bearing
$T_{\text{bo}}$	Temperature sensor of outer bearing
$T_{\text{R}}$	Temperature of rotor measured by thermal camera
$T_{\text{ph},0}$	Winding temperature at 20°C
$T_{\text{ph},n}$	New winding temperature
$T_{\text{uv}}$	Temperature sensor of uv phase
$T_{\text{vw}}$	Temperature sensor of vw phase

$T_{wu}$	Temperature sensor of wu phase
$\hat{T}$	Calculated temperature
$\hat{T}_m$	Measured temperature
$t$	Time
$u_d$	Voltage in the d-axis
$q_q$	Voltage in the q-axis
$u_s$	Stator voltage
$w$	Window width
$\vec{x}$	Unit vector
$x_n$	Averaged temperature
$\vec{y}$	Unit vector
$y_n$	Raw value of learning data
$\alpha_{Cu}$	Temperature coefficient of resistance
$\alpha$	Experimental coefficient
$\Delta P_{Cu}$	Stator copper losses
$\Delta P_{eddy}$	Eddy current losses
$\Delta P_{ex}$	Excess losses
$\Delta P_{hys}$	Hysteresis losses
$\Delta P_{mag}$	Stator magnetic losses
$\Delta P_{mech}$	Mechanical losses
$\Delta P_{rot}$	Rotor losses
$\Delta P_{tot}$	Total losses
$\Delta P_{\rho,2}$	Rotor end ring power losses
$\Delta R_{i,0}$	Values resistance by which is resistance at zero speed increased
$\Delta T$	Temperature difference

$\delta_s$	Load angle
$\delta$	Air gap thickness
$\delta(n)$	Delta distribution
$\epsilon$	Emissivity
$\epsilon$	Value of the residuum
$\theta$	angle between $B_r$ and x-axis
$\lambda$	Thermal conductivity
$\mu$	Dynamic viscosity of the coolant
$\nu$	Speed of inner air
$\rho$	Material resistivity
$\rho$	Density of the coolant
$\sigma$	Stefan-Boltzmann constant
$\varphi$	Angle between current and voltage
$\phi$	Overall radiation flow
$\phi_a$	Absorbed part of flux
$\phi_r$	Reflected part of flux
$\phi_{tr}$	transmitted part of flux
$\psi_D$	Damper winding flux linkage D-axis
$\psi_D$	Damper winding flux linkage
$\psi_d$	Flux linkage in the d-axis
$\psi_{PM}$	Permanent magnet flux linkage
$\psi_q$	Flux linkage in the q-axis
$\psi_Q$	Dumper winding flux in the q-axis
$\psi_S$	Total stator flux linkage
$\omega$	angular frequency of the shaft

$\omega_r$	Angular velocity of rotor
$\cos\varphi$	Power factor of machine

# List of appendices

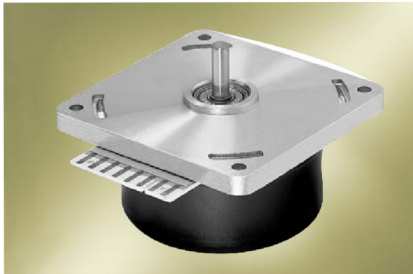
A Datasheet of analyzed machine

78

# A Datasheet of analyzed machine

## VARIODRIVE-Motor

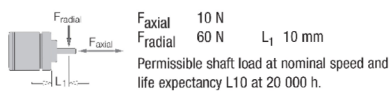
VD-3-54.14



- 3-phase, 6-pulse external rotor motor.
- EC technology.
- Dynamically balanced rotor with 4-pole, plastic-bonded ferrite magnet.
- Determination of rotor position via 3 Hall sensors.
- Motor supply and control via external operating electronics.
- Customer-specific winding layout and / or motor part sets available on request.

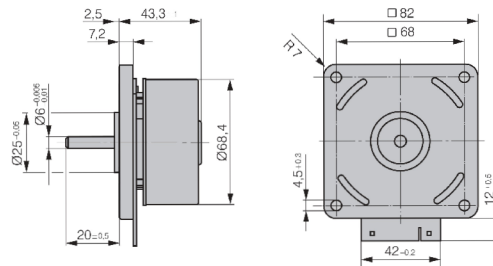
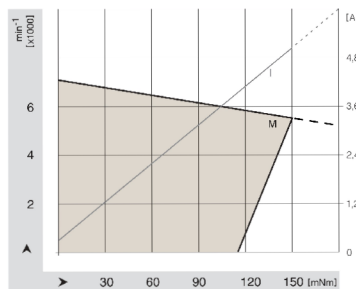
### Nominal Data

Type		VD-3-54.14	...010	...005
Nominal voltage ( $U_{BN}$ )	V DC	24	24	24
Nominal speed ( $n_N$ )	min <sup>-1</sup>	5 600	3 700	6 200
Nominal torque ( $M_N$ )	mNm	150	150	150
Nominal current ( $I_{BN}$ )	A	5.1	3.6	5.7
Nominal output power ( $P_N$ )	W	88	57	97
Free-running speed ( $n_0$ )	min <sup>-1</sup>	7 100	5 200	7 250
Free-running current ( $I_{0L}$ )	A	0.41	0.26	0.43
Permanent stall torque ( $M_{BND}$ )	mNm	115	115	135
Permissible eff. stall current, motor lead ( $I_{N0eff}$ )	A	4.4	3.1	5.4
Permissible permanent input power at stall ( $P_{BND}$ )	W	13	13	13
Short-term perm. peak torque ( $M_{max}$ )	mNm	400	400	440
Permiss. peak current, motor lead ( $I_{max}$ )	A	15	10	20
Induced voltage ( $U_{max}$ )	V/1000min <sup>-1</sup>	3.06	4.38	2.95
Terminal resistance	Ω	0.49	0.96	0.33
Terminal inductance	mH	1.00	2.00	0.72
Rotor moment of inertia ( $J_p$ )	kgm <sup>2</sup> x10 <sup>-6</sup>	145	145	165
Thermal resistance ( $R_{\theta}$ )	K/W	2.5	3.0	2.4
Protection class		IP 00	IP 00	IP 00
Ambient temperature range ( $T_{ij}$ )	°C	0 ... +40	0 ... +40	0 ... +40
Motor mass (m)	kg	0.52	0.52	0.52
Order No.		937 5414 000	937 5414 010	937 5414 005



### Operating electronics for speed-controlled operation:

for Order No. 937 5414 000 = DRIVECONTROL VT-A / Order No. 937 2501 001  
 for Order No. 937 5414 010 = DRIVECONTROL VT-A / Order No. 937 2501 002  
 for Order No. 937 5414 005 = DRIVECONTROL VT-D on request



ebmpapst

13